1980

The development of a bistatic electromagnetic scattering laboratory employing time domain measurement techniques for impulse response determination and target classification.

Hammond, Charles W., Jr.

Monterey, California. Naval Postgraduate School

http://hdl.handle.net/10945/17558

Maxwell - 160

NAVAL POSTGRADUATE SCHOOL

Monterey, California

THESIS

THE DEVELOPMENT OF A BISTATIC
ELECTROMAGNETIC SCATTERING LABORATORY
EMPLOYING TIME DOMAIN MEASUREMENT TECHNIQUES
FOR IMPULSE RESPONSE DETERMINATION
AND TARGET CLASSIFICATION

by

Charles W. Hammond, Jr.

December 1980

Thesis Advisor: M. A. Morgan

REPORT DOCUMENTATION PAGE		READ INSTRUCTIONS BEFORE COMPLETING FORM
1. REPORT NUMBER	2. GOVT ACCESSION NO.	3. RECIPIENT'S CATALOG NUMBER
4. TITLE (and Subtitle) The Development of a Bistatic Electromagnetic Scattering Laboratory Employing Time Domain Measurement Techniques for Impulse Response Determination and Target Classification		5. TYPE OF REPORT & PERIOD COVERED Master's Thesis; December 1980
		6. PERFORMING ORG. REPORT NUMBER
7. AUTHOR(s) Charles W. Hammond, Jr.		8. CONTRACT OR GRANT NUMBER(s)
9. PERFORMING ORGANIZATION NAME AND ADDRESS Naval Postgraduate School Monterey, California 93940		10. PROGRAM ELEMENT, PROJECT, TASK AREA & WORK UNIT NUMBERS
11. CONTROLLING OFFICE NAME AND ADDRESS Naval Postgraduate School Monterey, California 93940		12. REPORT DATE December 1980
		13. NUMBER OF PAGES 110
14. MONITORING AGENCY NAME & ADDRESS(if different from Controlling Office)		15. SECURITY CLASS. (of this report) UNCLASSIFIED
		15a. DECLASSIFICATION/DOWNGRADING SCHEDULE

16. DISTRIBUTION STATEMENT (of this Report)

Approved for public release; distribution unlimited

17. DISTRIBUTION STATEMENT (of the abstract entered in Block 20, if different from Report)

18. SUPPLEMENTARY NOTES

19. KEY WORDS (Continue on reverse side if necessary and identify by block number)

Time Domain Electromagnetic Scattering; Transient Scattering; Impulse Response, Transient Response; TEM Horn Antenna

20. ABSTRACT (Continue on reverse side if necessary and identify by block number)

A time domain measurements, electromagnetic scattering laboratory has been developed to provide a means of experimentally measuring the transient, scattered electromagnetic fields from symmetric objects for impulse response determination or target classification. The evolution of the physical laboratory is described in terms of the development of the transmitting and receiving antennas, the interface of the data processing hardware, the signal processing scheme, the software routine functions, and the fabrication of

scattering range targets.

The smoothed impulse response of a thin wire scatterer is experimentally determined, and a comparison of these measurements is made to a theoretical calculation of the response.

Approved for public release; distribution unlimited

The Development of a Bistatic Electromagnetic Scattering Laboratory Employing Time Domain Measurement Techniques For Impulse Response Determination and Target Classification

by

Charles W. Hammond, Jr.
Captain, U. S. Marine Corps
B.S., United States Naval Academy, 1971

Submitted in partial fulfillment of the requirements for the degree of

MASTER OF SCIENCE IN ELECTRICAL ENGINEERING

from the

NAVAL POSTGRADUATE SCHOOL
December 1980

ABSTRACT

A time domain measurements, electromagnetic scattering laboratory has been developed to provide a means of experimentally measuring the transient, scattered electromagnetic fields from symmetric objects for impulse response determination or target classification. The evolution of the physical laboratory is described in terms of the development of the transmitting and receiving antennas, the interface of the data processing hardware, the signal processing scheme, the software routine functions, and the fabrication of scattering range targets.

The smoothed impulse response of a thin wire scatterer is experimentally determined, and a comparison of these measurements is made to a theoretical calculation of the response.

TABLE OF CONTENTS

LIST OF FIGURES

I. INTRODUCTION

A. BACKGROUND

Since the early nineteen sixties, research in time domain or transient electromagnetics has continued to expand into new areas of application. Current research involving transient electromagnetics includes wide-band radar design, aircraft and missile radar cross section reduction, as well as the evaluation of the vulnerability of ships, aircraft, and ground installations to high level nuclear electromagnetic pulse (EMP) phenonmena. A direct time domain transient solution to an electromagnetic interaction problem can offer physical insight not readily apparent from a solution obtained by classical frequency domain techniques. Reasons to support this are that the scattering impulse response of an object is related to its geometrical configuration; the radar cross section can be obtained from the impulse response by a Fourier Transform, and the scattering response of an object to any waveform may be obtained from the impulse response by convolution.

As a practical application, advances in radar target identification brought forth by using transient response techniques could be profound, indeed. Consider, for example, the military and commercial impact if a radar operator could positively identify a radar return on his indicator as an

F-4 or MIG-21 aircraft and, in addition, also be able to determine the load configuration such as missiles, bombs, external fuel tanks, or electronic countermeasures gear. This idea is conceivable with advances in wide-band radar technology based on transient electromagnetics principles.

Generating an electronic signal which approximates an impulse was not possible until recent developments in subnanosecond pulse technology. This, coupled with the advances achieved in high speed digital processing, gave impetus to the evolution of the methodology necessary to solve the transient problem. Baum introduced the Singularity Expansion Method (SEM) in 1971. SEM is based on an extension of the Heaviside expansion theorem, used in circuit theory, brought into the realm of electromagnetic fields. The motivation behind most work in SEM has been the determination of EMP threat levels in military electronic hardware. SEM represents the currents induced on the scatterer as the real part of a series of complex exponentials such that

$$f(t) = \mathrm{Re}\{ \sum_{n=1}^{N} R_n \exp(js_n t)\} \qquad (1)$$

where R_n is the amplitude of each mode of a complex frequency s_n [Ref. 1]. References 2 through 4 address current research in this area.

In many cases, such as in radar target identification, the surface currents on the target are of importance only in the context of generating the scattered fields. Another approach to the problem is the Finite Element Method (FEM) described in Ref. 5. This method offers a direct solution of the scattered electromagnetic field as opposed to analysis of surface currents. Although the approaches are different, the final results are similar since the scattered fields are related to the surface currents by Maxwell's equations.

B. GENERAL GOALS

In order to study transient electromagnetics and to exercise the methods previously discussed, facilities must be provided for experimentation. With this idea, the Naval Postgraduate School Time Domain Measurements Laboratory was developed. This laboratory provides a means of obtaining time domain measurements of the transient scattering response of an object to incident signals produced by voltage pulses or steps applied to a transmitter antenna and reflected from the target. The laboratory was constructed primarily to measure the transient scattered field from plane-symmetrical objects for impulse response determination and target classification. This is consistent with the long range goal which is to provide a means which will ultimately establish the feasibility of developing advanced radar systems which

are capable of target discrimination and classification via time domain scattering analysis. In addition, research in radar cross section modeling and nuclear EMP vulnerability is also underway which extend the scope of the original project.

C. FINAL PHYSICAL LABORATORY DESCRIPTION

Figure 1 shows the physical configuration of the laboratory. A block diagram of the scattering range is shown in Figure 2. The signal source is a mercury reed switch type pulse generator which produces a 250 picosecond risetime voltage pulse of calibrated amplitude and variable pulse width. The incident pulse is sent through 50 ohm coaxial cable and a 60 nanosecond delay line to a twenty-one foot monopole transmitting antenna protruding through the aluminum image plane. The image plane isolates the transmitting and receiving antennas from the electronic equipment below. The incident electromagnetic field radiates outward from the transmitting antenna. This field illuminates a target on the image plane, and subsequently, the target reradiates a scattered electromagnetic field. The incident field, as well as the scattered field, are received by the Transverse Electric and Magnetic (TEM) horn antenna. The received signal is routed through a 50 ohm coaxial cable to a digital processing oscilloscope (DPO) that has been triggered by a portion of the signal from the pulse generator. The received signal is sampled in the DPO, then

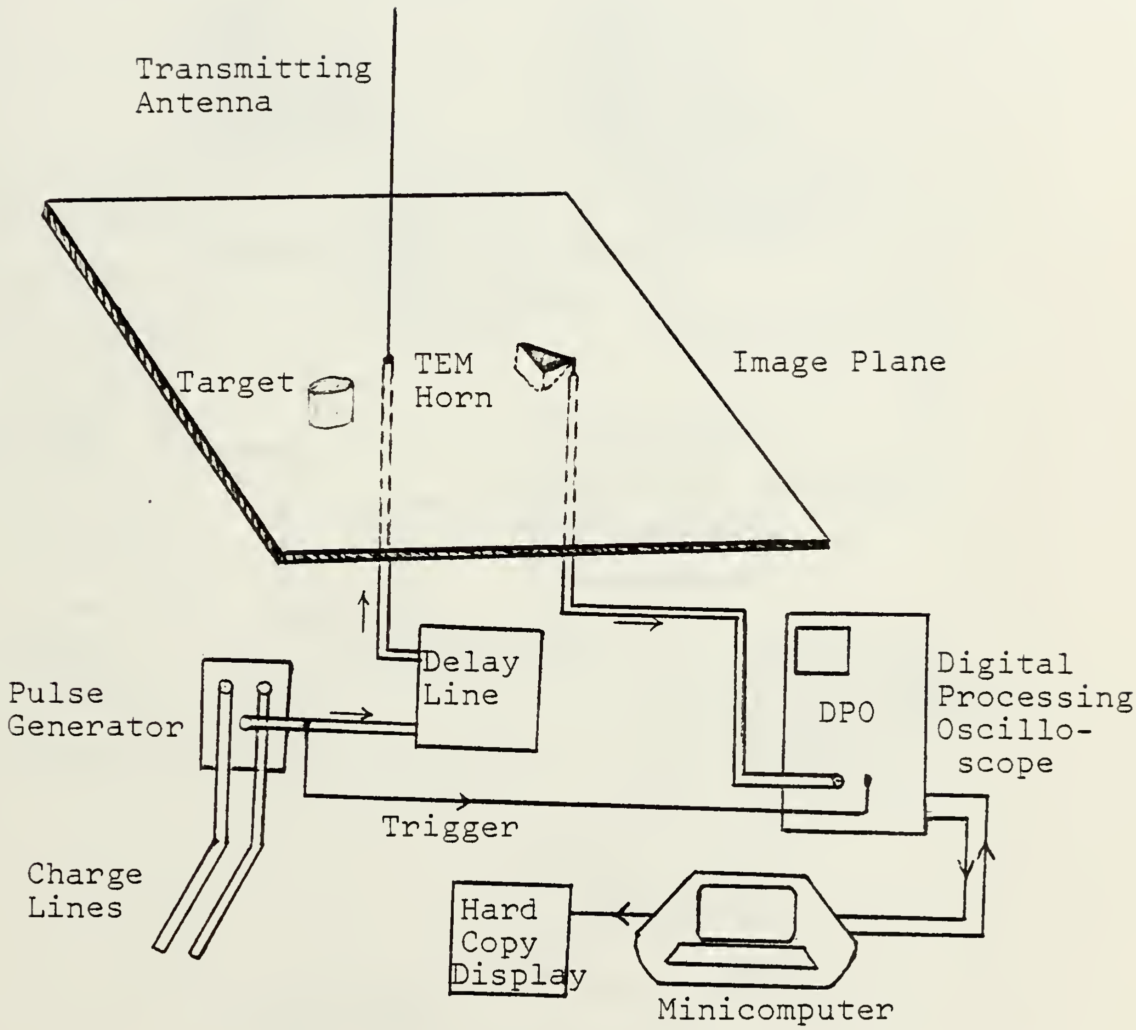

Figure 1. Experimental Configuration of Scattering Range

Figure 2. Block Diagram of Scattering Laboratory

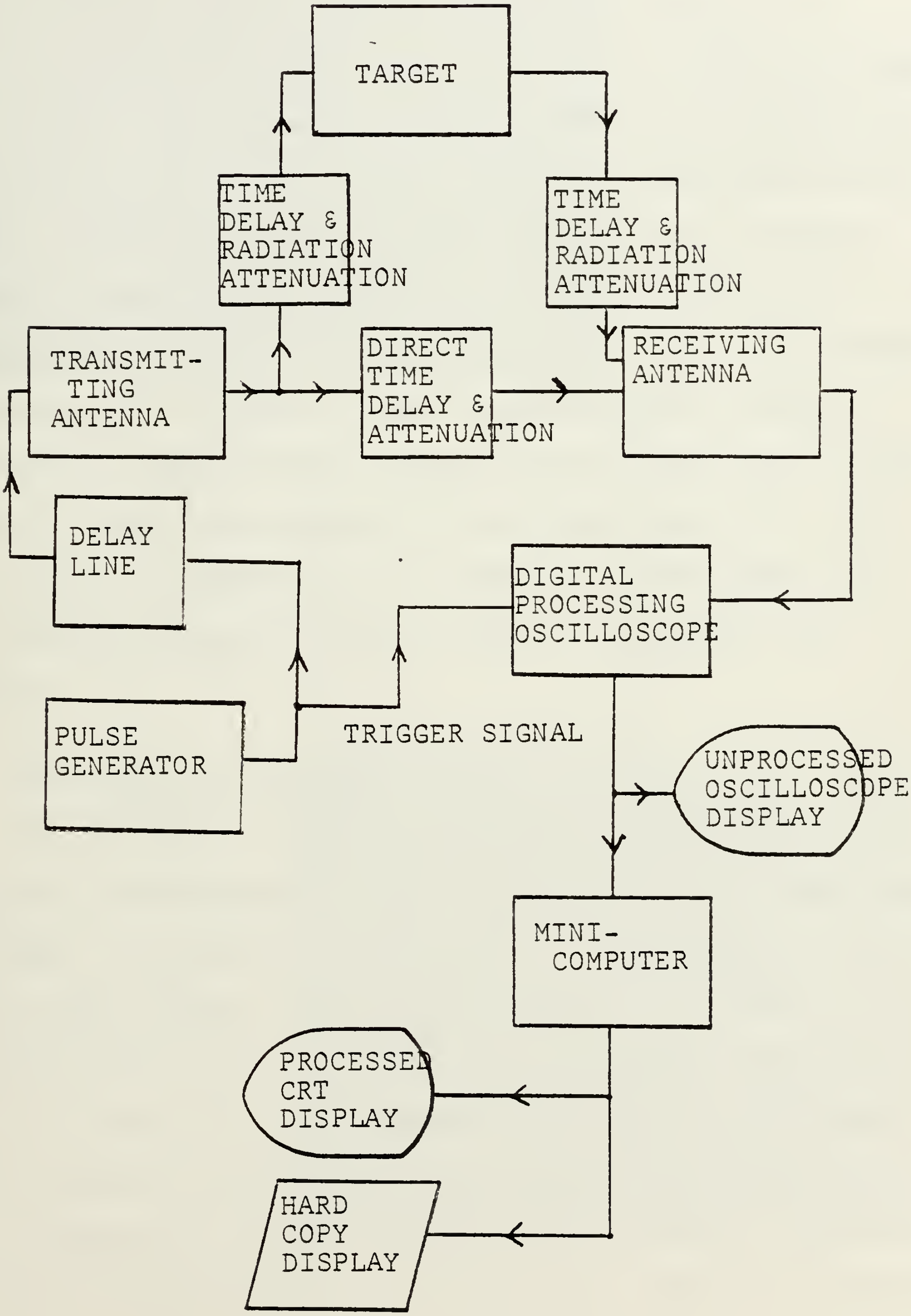

transferred to a minicomputer for storage and further signal processing. Figure 3 shows the response with no targets on the image plane to a 50 volt amplitude pulse of 20 nanosecond pulse width at the oscilloscope before any signal processing. This compares very favorably with the results in reference [6]. The display shows a 20 nanosecond time window between the direct transmission and the erratic response caused by the end of the incident pulse and reflections from the tip of the antenna. This time window is convenient to view a target response since unwanted reflections can be gated out in time with the oscilloscope. Figure 4 shows the response to the same input pulse with two conically shaped metallic targets on the image plane. The target response is seen in the 20 nanosecond time window.

D. MEASUREMENT PROCEDURE

The response in Figure 4 contains the superpositioned incident electromagnetic field and the scattered field from a target. In addition, the waveform is impregnated with noise from internal and external sources. In order to determine the transient response of a target, the noise must be reduced to an acceptable level, and the incident electromagnetic field must be subtracted from the signal. In any sequence of measurements of the transient response, certain procedures must be carried out. First, the incident

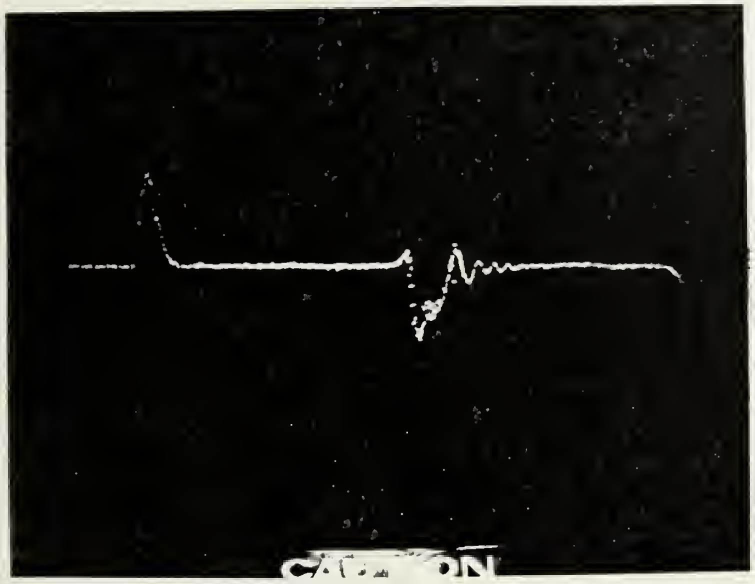

Figure 3.
Response to 50
Volt Amplitude.
20 nanosec Wide
Pulse

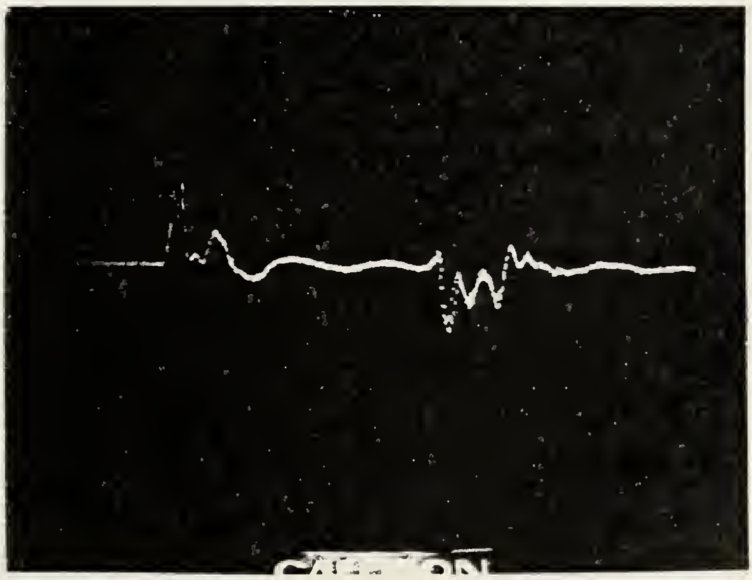

Figure 4.
Response of 2
Conical Targets
to a 50 Volt,
20 nanosec Wide
Incident Pulse

signal is measured without a target on the image plane. Results similar to Figure 3 should be obtained. N successive incident signals are transmitted from the monopole antenna, received by the TEM horn antenna, sampled by the DPO, and transferred to the minicomputer. There a running summation of the incoming waveforms is tallied until all of the N signals have been processed. A time-average of the sampled data set of incident waveforms is computed by the equation

$$A1(k) = \frac{1}{N} \sum_{i=1}^{N} A_i(k) \qquad k=1,2,\ldots 512 \qquad (2)$$

where $A_i(k)$ is the ith waveform transferred from the digital processing oscilloscope. The value of N is made large enough to sufficiently reduce the noise level, as will be discussed in Chapter II, Section C.

Next, a target is placed on the image plane at a particular distance and aspect angle from the antennas. Once again N successive signals are processed as before, then a time-average, B1(k), is computed using equation (2) for the sampled data set of waveforms containing both the incident signal and the scattered response. These waveforms will be referred to as "augmented waveforms".

To remove the incident signal from the augmented waveform, a difference C(k) is found by

$$C(k) = B1(k) - A1(k) \qquad k=1,2,\ldots\ldots,512 \qquad (3)$$

C(k) represents the sampled target response convolved with the transient responses of the transmitting and receiving antennas.

II. SCATTERING LABORATORY DEVELOPMENT

A. CONSTRUCTION OF PROTOTYPE MODELS

The development of the present scattering laboratory was based on knowledge attained from two earlier prototype laboratories constructed during this endeavor. In the development of the first model, learning the principles of scattering range operation and the essentials of equipment interface were the paramount goals. In the second prototype, proper antenna selection was the primary consideration.

The first model consisted of a 22cm x 22cm aluminum image plane with two straight, copper wire antennas protruding through, as shown in Figure 5. The center wire antenna was used to transmit the incident signal from the pulse generator. The receiving antenna was placed in the corner of the image plane and connected by coaxial cables to the sampler head of the sampling oscilloscope. Figure 7 shows the response to a 37.5 volt, incident step pulse with a 10 nanosecond pulse width, Figure 6. In reference 7, a similar configuration is described, and the results in both cases are similar.

The initial model proved that the electronic equipment could be satisfactorily interfaced to produce an interaction between the two antennas; however, several factors inherent with this model made quantitative analysis of the

Figure 5. First Prototype Scattering Range Model

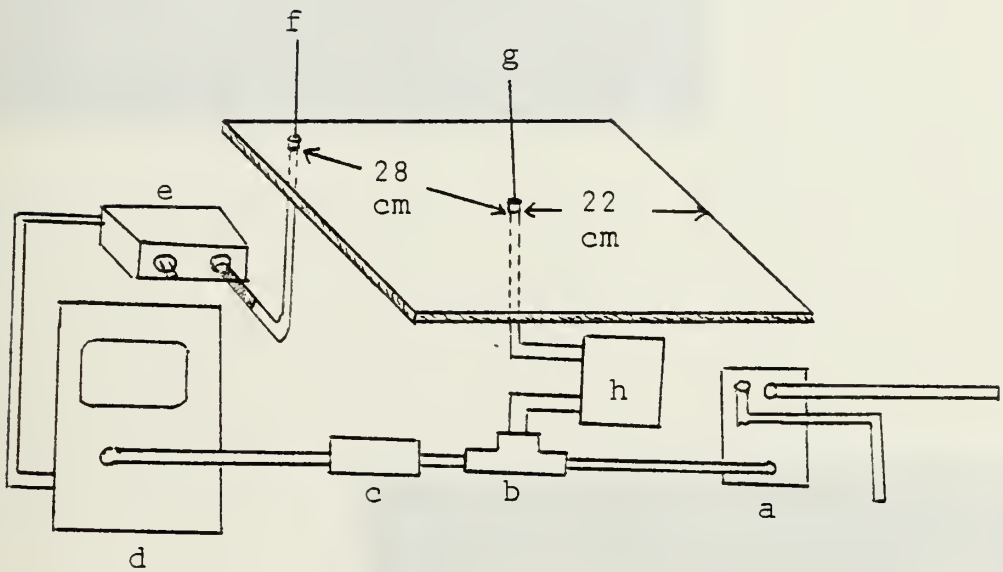

a. pulse generator
b. power divider
c. 10x attenuator
d. sampling oscilloscope
e. sampler head
f. receiving antenna
g. transmitting antenna
h. 60 nsec delay line

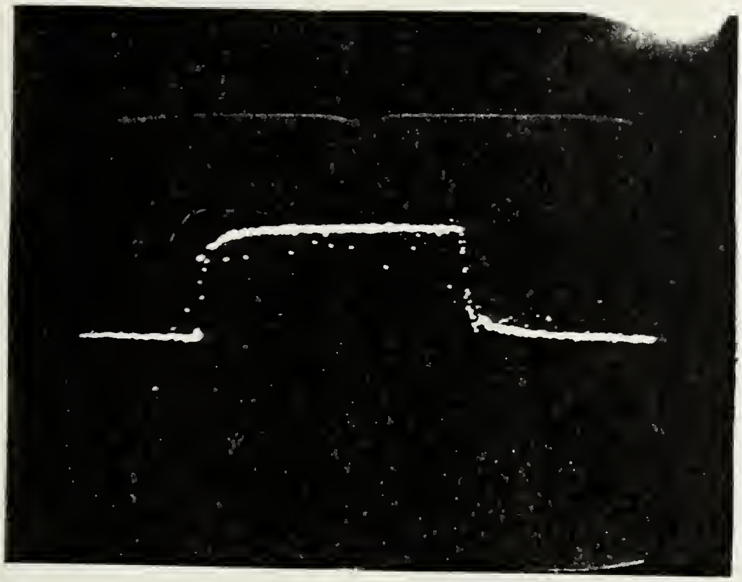

Figure 6,
37.5 Volt 10 nsec
Pulse Width,
Incident Pulse.

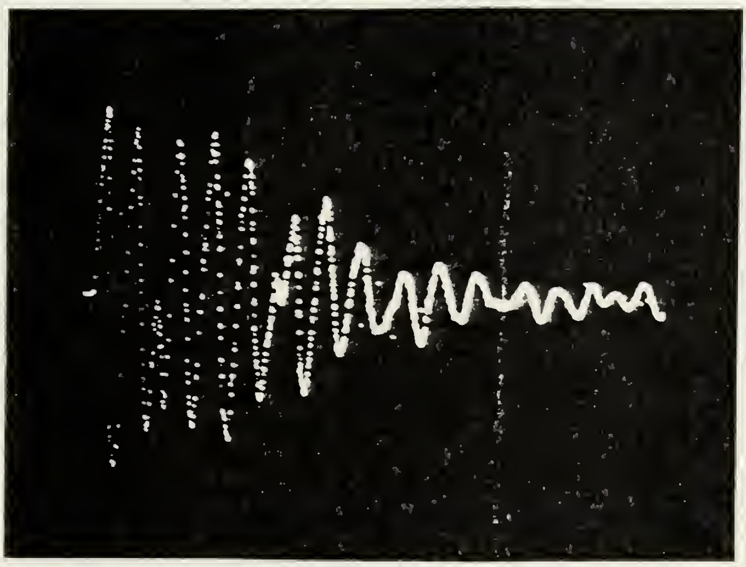

Figure 7.
Response to
37.5 Volt Amplitude 10 nsec
Pulse Width
Incident Pulse
(figure 6)

response difficult. These factors were related to the small size of the image plane and the close proximity of the antennas.

To overcome these problems, a larger model was constructed. In the second model, a longer transmitting antenna was used, and two broadband receiving antennas were tested to improve the quality of the response. The equipment interface below the image plane was essentially identical to the first model.

The length of the transmitting antenna was increased to 182 cm. The travel time for a pulse to reach the tip of the antenna and be reflected was approximately 6 nanoseconds. This provided a longer time window on the oscilloscope display before unwanted reflections appeared in the signal.

Two receiving antenna designs were tested. The first antenna was a coaxial cone antenna (Figure 8). Experimental and theoretical descriptions are contained in reference 8. The received response of this antenna to an incident field is a differentiation with respect to time. This type of response is useful in scattering work when the radiated field is a step function in time.

Another antenna design in the literature is the TEM horn antenna. Analyses in the frequency and time domains are found in references 9 and 10. The TEM horn antenna can be viewed as a pyramidal horn with open sides. See Figure 9.

Figure 8. Coaxial Cone Antenna

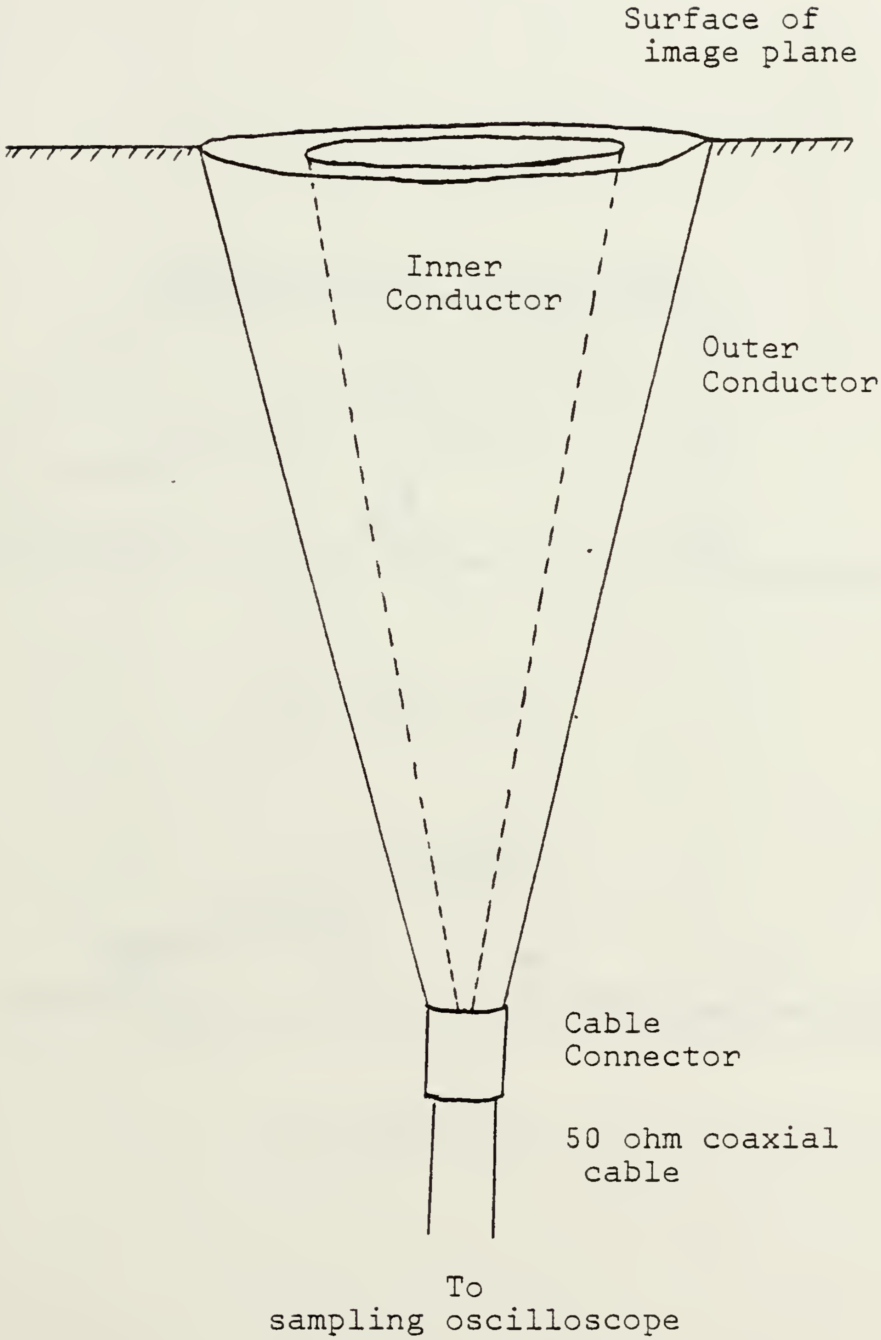

Figure 9. TEM Horn Receiving Antenna

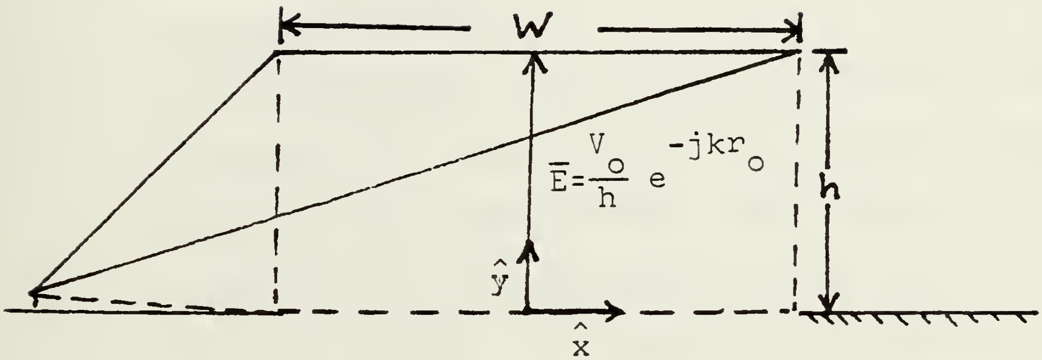

(a) Front View

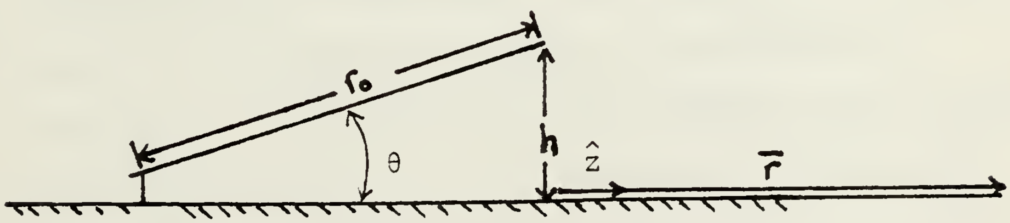

(b) Side View

If the horn flare angle θ and the plate width W are chosen properly, a constant characteristic impedance can be obtained.

The TEM horn antenna was selected for use in the scattering laboratory. Factors influencing the choice were:

1. BETTER DIRECTIVITY. The TEM horn antenna can be directed at a target anywhere on the image plane to maximize reception.
2. LESS ANTENNUATION. The TEM horn antenna had less attenuation than the coaxial cone antenna tested.
3. MOBILITY ON THE IMAGE PLANE. The TEM horn antenna is much easier to move around on the image plane due to its design. The coaxial cone antenna must remain in a fixed position on the range flush with the image plane.
4. CHARACTERISTIC IMPEDANCE. The characteristic impedance of the TEM horn antenna is adjusted by changing the flare angle. The coaxial cone antenna requires redesign of the dimensions to alter the characteristic impedance.

Having made the receiving antenna selection, Figure 10 shows the final configuration of the second model. When a 35 volt amplitude pulse with a 20 nanosecond pulse width was applied to the transitting antenna, the response in Figure 11 was obtained. Although the results did not match

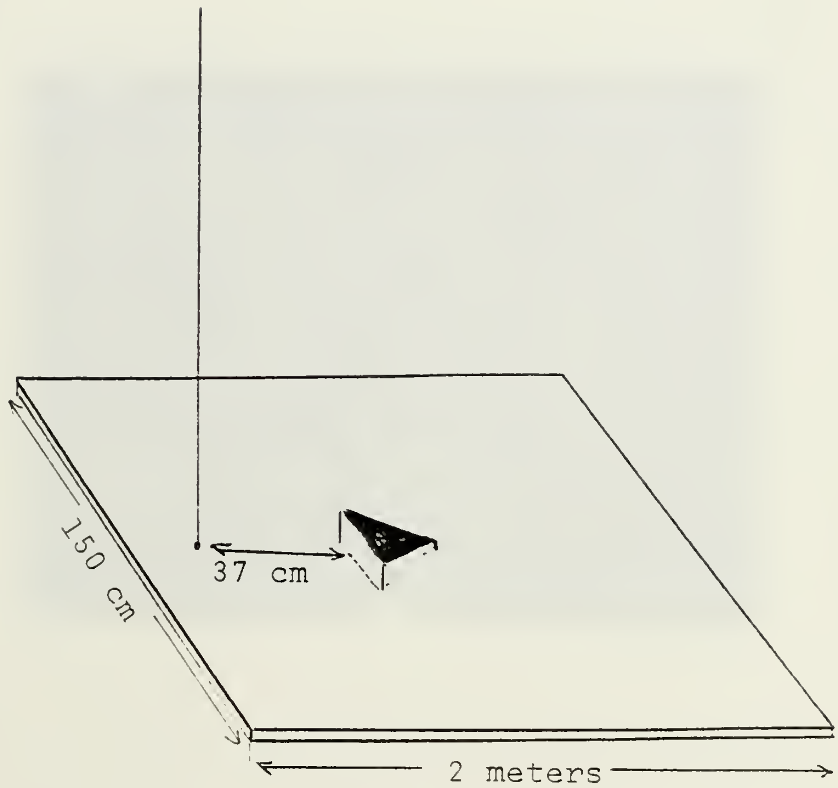

Figure 10. The Second Prototype of Scattering Range Model (Image Plane Configuration Only)

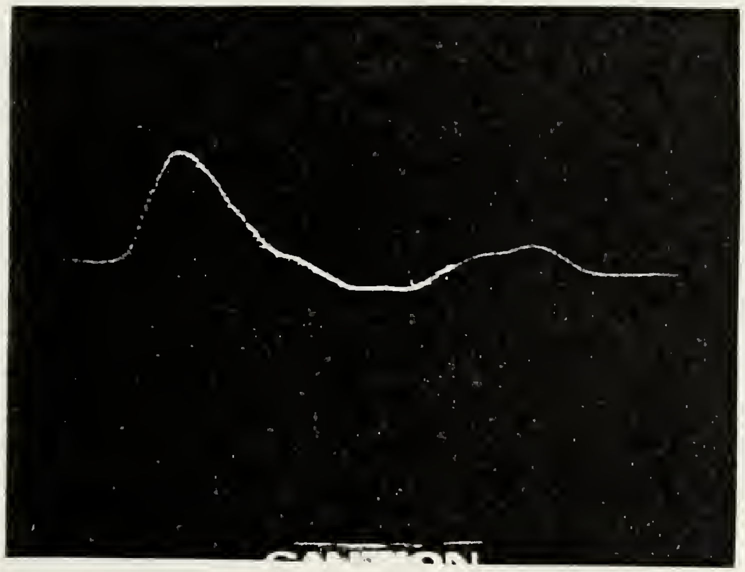

Figure 11. Second Prototype Scattering Range Model. The Response to a 35 Volt, 20 nanosec Pulse Wide Incident Pulse.

those in Figure 3 and in reference 6, there were fewer oscillations than in the first model indicating the TEM horn is a satisfactory receiving antenna.

B. ANTENNA DEVELOPMENT

1. Receiving Antenna

Having made the preliminary receiving antenna selection heuristically, a theoretical approach was pursued to investigate the transmitting and receiving characteristics of the TEM horn antenna as depicted in Figure 9. It was assumed that the flare angle θ and the plate width W were chosen so that the characteristic impedance is approximately constant and only the TEM mode propagates in the horn. Edge diffraction and fringing fields are neglected. The field at the aperture is thus given by the TEM wavefront

$$E_y(x,y,0) = \frac{V_o}{h} e^{-jkr_o} \qquad (4)$$

where V_o is the amplitude of the incident voltage at the feedpoint, h is the height of the aperture, and k is the wave number $2\pi/\lambda$. The $\overline{E}$ field closely approximates the spherical wave assumed in reference [10]. Knowing the field at the aperture, equivalent magnetic currents are found from Harrington, reference 11, by

$$\overline{M} = 2\overline{E} \times \hat{n} \tag{5}$$

thus

$$M_x = \frac{2V_o}{h} e^{-jkr_o} \tag{6}$$

The electric vector potential $\overline{F}$ is given by

$$\overline{F} = \frac{1}{4\pi} \int\int_{aperture} \overline{M} \frac{e^{-jkr}}{r} ds \tag{7}$$

where r is the distance from the aperture to an observer on the image plane in the boresight direction. In the far-zone of the aperture $\overline{F}$ then becomes

$$F_x = \frac{V_o W e^{-jk(r+r_o)}}{2\pi r} \tag{8}$$

The far-zone radiation fields form a TEM wave which are related to the electric vector potential by

$$H_x = -jw\varepsilon_o F_x \tag{9}$$

$$E_y = \eta_o H_x = -jw\varepsilon_o \eta_o F_x \tag{10}$$

where $\eta_o = 120\pi$ ohms is the characteristic impedance of free space. The radiated fields become

$$H_x^{rad} = \frac{V_o We^{-jk(r+r_o)}}{2\pi r} \cdot (-jw\varepsilon_o) \qquad (11)$$

$$E_y^{rad} = \frac{-j60w\varepsilon_o V_o We^{-jk(r+r_o)}}{r} \qquad (12)$$

The transmitting transfer function is given in reference 9 by

$$S_t(f) = \frac{\bar{E}^{rad}(f)}{V_o(f)} = \frac{-j60\ F(f)e^{-jkr}}{[Z_o(f)+Z_g(f)]r} \qquad (13)$$

where F(f) is the radiation function, $Z_o(f)$ is the input impedance of the horn, and Zg(f) is the generator impedance. Using equation 12, $S_t(f)$ becomes

$$S_t(f) = \frac{-j60\ (2\pi f)\varepsilon_o We^{-jk(r_o+r)}}{r} \qquad (14)$$

When simplified, (14) becomes in terms of F(f)

$$F(f) = Z_o(f)+Z_g(f)\quad -2\pi f\varepsilon_o We^{-jkr_o} \qquad (15)$$

Assuming the load impedance Z_L and the generator impedance $Z_g(g)$ are real and equal, the Rayleigh-Carson reciprocity theorem in reference 12 provides that

$$F(f) = -h_e(f)k \qquad (16)$$

By using (16) the effective height, $h_e(f)$, becomes

$$h_e(f) = \frac{2\pi f \varepsilon_o W e^{-jkr_o}(Z_o(f)+Z_g(f))}{k} \tag{17}$$

The receiving transfer function, $S_r(f)$, can be determined with the aid of reference 9 as

$$S_r(f) = \frac{V_L(f)}{\bar{E}^{inc}(f)} = \frac{h_e(f)Z_L}{Z_o(f)+Z_L} \tag{18}$$

Substituting equation (17) into (18) leads to

$$S_r(f) = -c\varepsilon_o W z_L e^{-jkr_o} \tag{19}$$

Taking the inverse Fourier transform, where

$$s(t) = \int_{-\infty}^{\infty} S(f)e^{j2\pi ft}df \tag{20}$$

the receiving transfer function, $S_r(f)$, gives

$$s_r(t) = -c\varepsilon_o W z_L \delta(t-r_o/c) \tag{21}$$

while the transmitting transfer function, $S_t(f)$, in (14) yields the transmitting impulse response

$$s_t(t) = -\frac{60\varepsilon_o W}{\bar{r}} \frac{\partial}{\partial t} \delta\,(t-r_o/c) \tag{22}$$

Comparing (21) and (22) shows that the transmitting impulse response is simply the time derivative of the receiving impulse response. This is in agreement with the results in reference [10].

Consider equation (21). The impulse response is an impulse, delayed in time by r_o/c, multiplied by a negative constant which is dependent on the width of the antenna aperture, W, and the load impedance, z_L. This theoretical result can be accepted if it can also be shown to be experimentally valid.

The far-zone field step response of a linear dipole antenna is computed in references 7 and 13. If the step response of a dipole antenna, as measured by the voltage output of the TEM horn antenna, is comparable to the theoretical transmitted field results in references 7 and 13, then two implications follow: first, the TEM horn is apparently in the far field of the dipole, and second, the TEM horn produces negligible dispersion and distortion of the received signal. Thus equation (21) can be verified.

A one meter, wire monopole antenna; equivalent to a two meter, dipole antenna; was constructed on the image plane. (The 7 meter long transmitting monopole antenna was removed.) The meter long antenna was center-fed with a smoothed step, incident signal from the pulse generator. Figure 12a depicts the driving voltage measured at the antenna feedpoint. The augmented signal in Figure 12b is

Figure 12. WAVEFORM STATISTICS

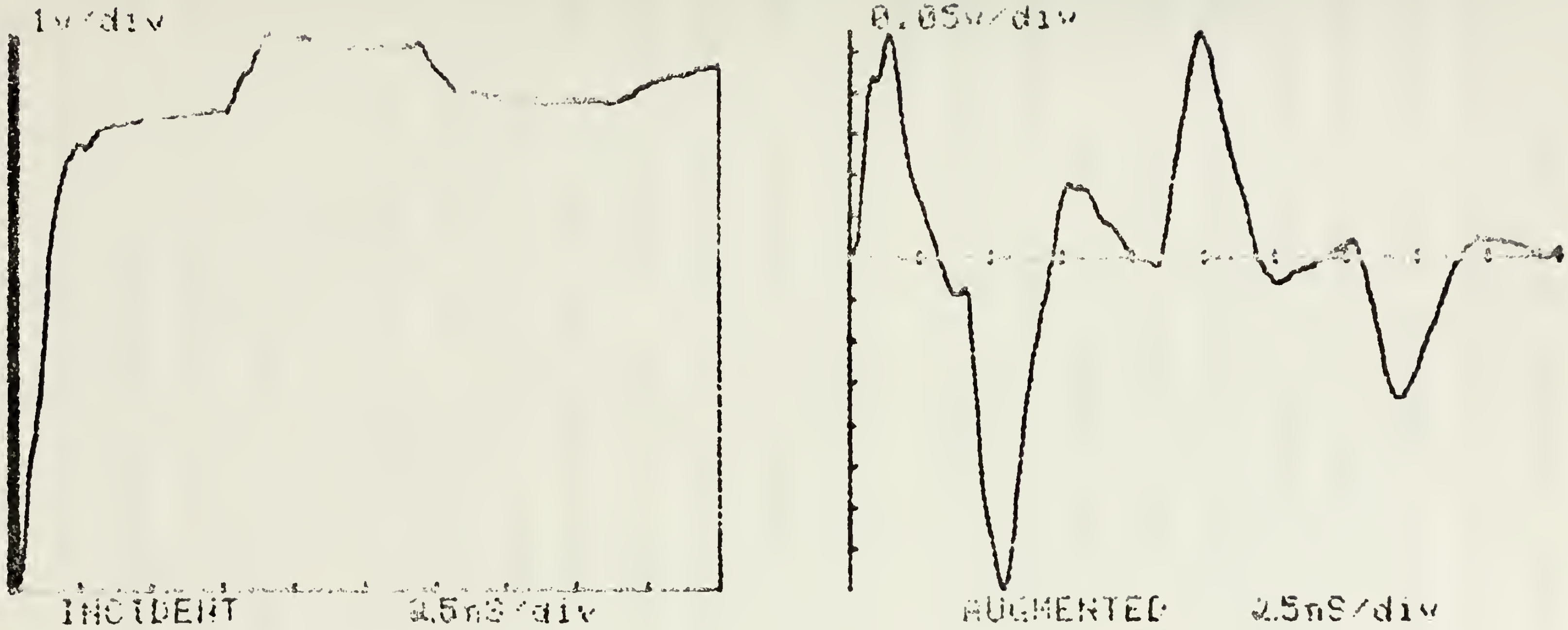

(a) (b)

FOR N= 59

	INCIDENT	AUGMENTED
MAXIMUM PEAK VALUE (VOLTS)	162.6074	0.2731
MINIMUM VALUE (VOLTS)	0.0000	-0.3969
RMS VALUE (VOLTS)	101.0782	0.0910
MEAN VALUE (VOLTS)	69.9730	0.0010

the two meter dipole response measured by the TEM horn antenna at a distance of 270 cm and at a broadside angle of incidence. Using the signal processing software routine described in Chapter II, Section E, the impulse response of the dipole antenna was computed through the use of fast fourier transforms and the inverse fourier transform. The impulse response, shown in Figure 13, was integrated with the use of a signal processing read only memory (ROM) described in Chapter II, Section D. Integration of the impulse response yields the step response of the coupled antennas, Figure 14.

This experimentally obtained step response was compared to the results in reference 13. There were two factors which caused the experimental and theoretical results to differ. First, the experimental step response lagged the theoretical step response in time; second, the experimental voltage and a reversed polarity compared to the theoretical field. Both the time delay and the negative factor are contained in equation (21), and hence are attributable to the properties of the TEM horn antenna. Agreement between the two results is quite good. See Figure 15. This validates the assumptions used to establish (21), thus making (21) a reasonable representation for the impulse response of the TEM horn antenna.

Figure 13. IMPULSE RESPONSE OF 1m PIPE AND TEN HORN

Figure 14. TDR RESPONSE OF 1m WIRE AND TEM HORN

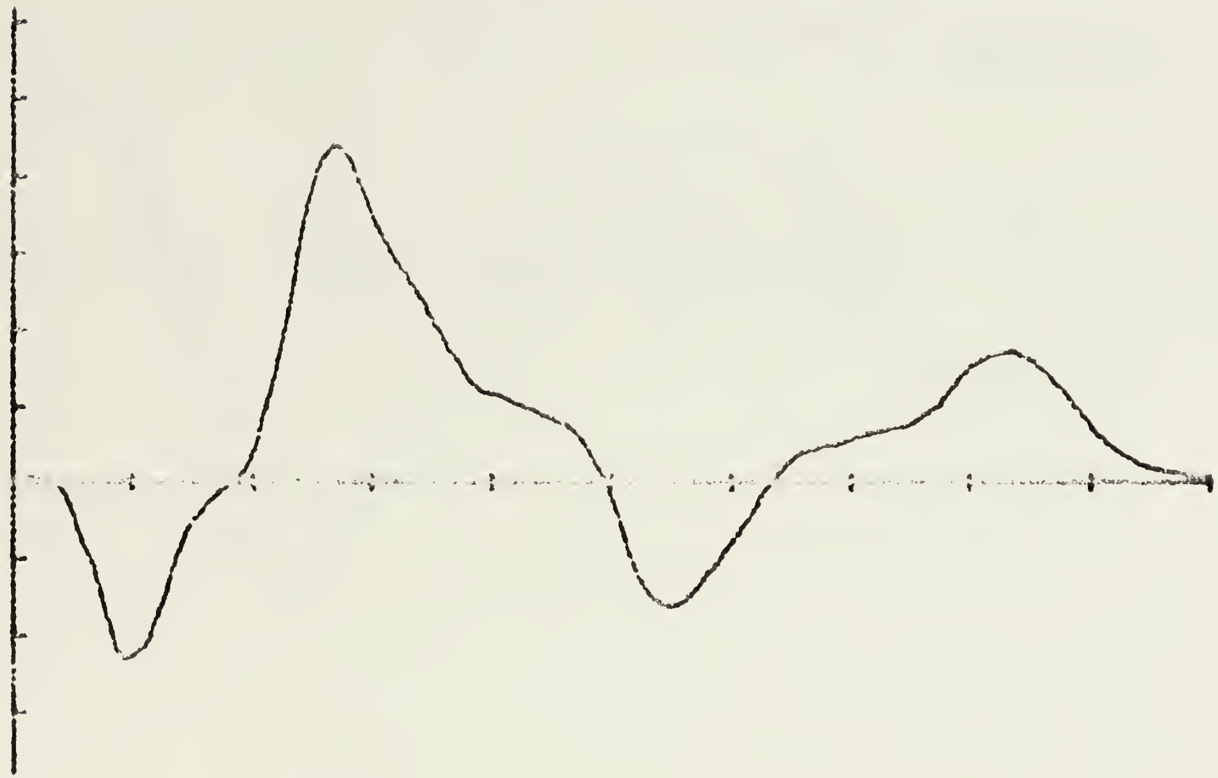

Figure 15. Comparison of Theoretical Far Zone Field Step Response and Experimental Step Response of Dipole Antenna

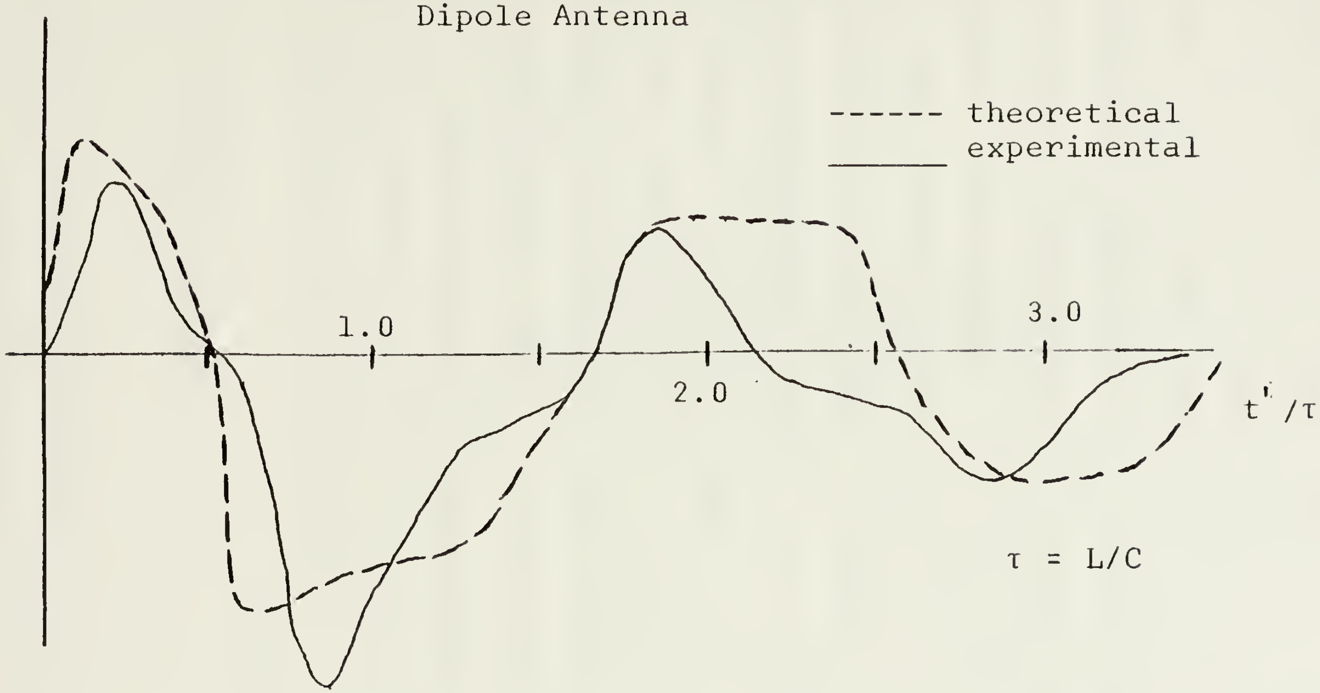

2. Transmitting Antenna

The implication of equation (21) is that a receiving signal waveform will be guided through the TEM horn antenna without distortion. Although this is not completely true, since there will be some losses, dispersion, and distortion due to impedance mismatches and multiple modes, this assumption was used to experimentally determine the impulse response of the transmitting antenna. By disconnecting the coaxial cables at the transmitting and receiving antennas and reconnecting the cables as shown in Figure 16, the input signal x(t) to the transmitting antenna can be measured directly. Figure 17a shows the incident signal to be a smoothed step function with approximately a 250 picosecond risetime. The trailing edge of the pulse was time windowed out using the sampling oscilloscope. When the cables were reconnected as in Figure 1, the response y(t) was measured and is shown in Figure 17b. This response is related to the incident signal by the double time convolution

$$y(\tau) = [h(t) * s_r(\tau)] * x(t)$$

where h(t) is the impulse response of the transmitting antenna, $s_r(\tau)$ is the receiving impulse response of the TEM horn antenna, and $\tau = t - r_o/c$ is the time delay. Taking the magnitude of the Fourier transform of $y(\tau)$ yields

$$|Y(f)| = |H(f)S_r(f)||X(f)| \tag{23}$$

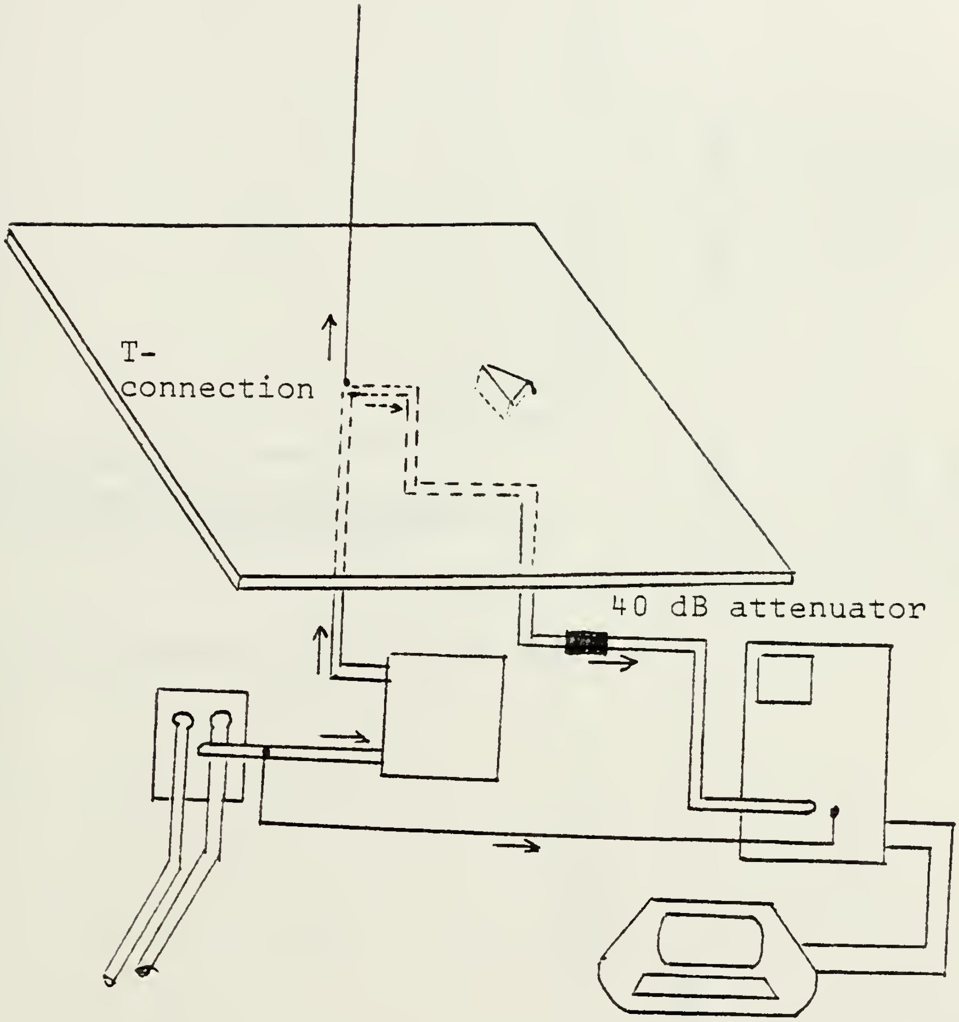

Figure 16. Coaxial Cable Connection Used to Measure Incident Pulse

Figure 17. [illegible]AVEFORM STATISTICS

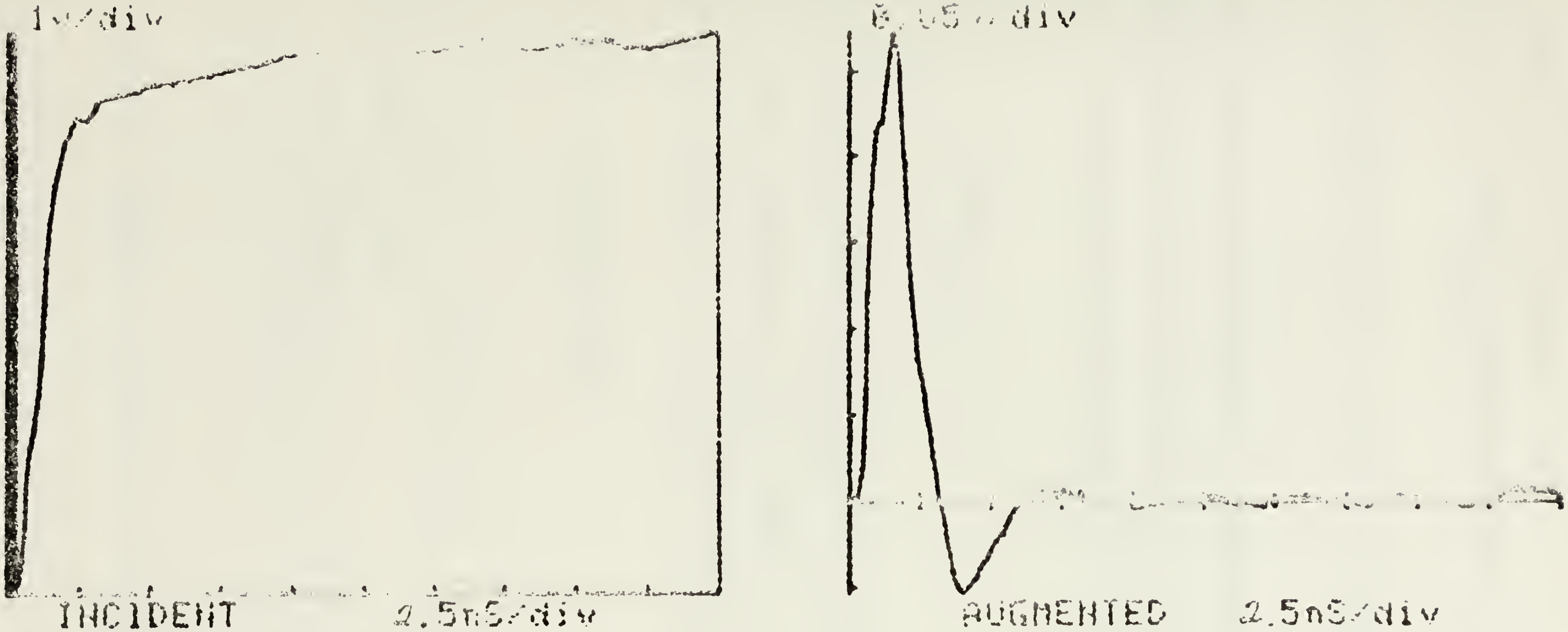

(a) (b)

FOR N= 50

	INCIDENT	AUGMENTED
MAXIMUM PEAK VALUE (VOLTS)	[illegible]8.5762	0.2726
MINIMUM VALUE (VOLTS)	0.0000	-0.0525
RMS VALUE (VOLTS)	1[illegible]8.2588	0.0485
MEAN VALUE (VOLTS)	74.9713	0.0068

The magnitude and phase plots of Y(f) and X(f) are shown in Figure 18. Dividing these results gives

$$|G(f)| \triangleq |H(f)S_r(f)| = |Y(f)|/|X(f)| \tag{24}$$

Taking the inverse Fourier transform of (24) yields an expression g(t) for the convolved transient impulse responses of the transmitting and receiving antennas such that

$$g(t) = h(t)*s_r(t) \tag{25}$$

Using (21) and the results of the experimental determination of the step response of the dipole, g(t) represents the impulse response of the transmitting antenna such that

$$g(\tau) = -(c\varepsilon_o W z_L)h(t) \tag{26}$$

where $\tau = t - r_o/c$. Figure 19 shows the experimentally determined value of $g(\tau)$.

From reference 14, the time domain, electromagnetic, far-zone fields transmitted by a wire antenna are given by

$$\overline{H}(\overline{r},t) = \frac{1}{4\pi rc} \int_s \frac{\partial}{\partial \tau} \overline{J}_s (r',\tau) x \frac{\overline{r}}{|r|} ds' \tag{27}$$

$$\overline{E}(\overline{r},t) = \eta_o \overline{r} \text{ x } \overline{H}(r,t) \tag{28}$$

FFT OF THE [illegible] AND AUGMENTED [illegible]

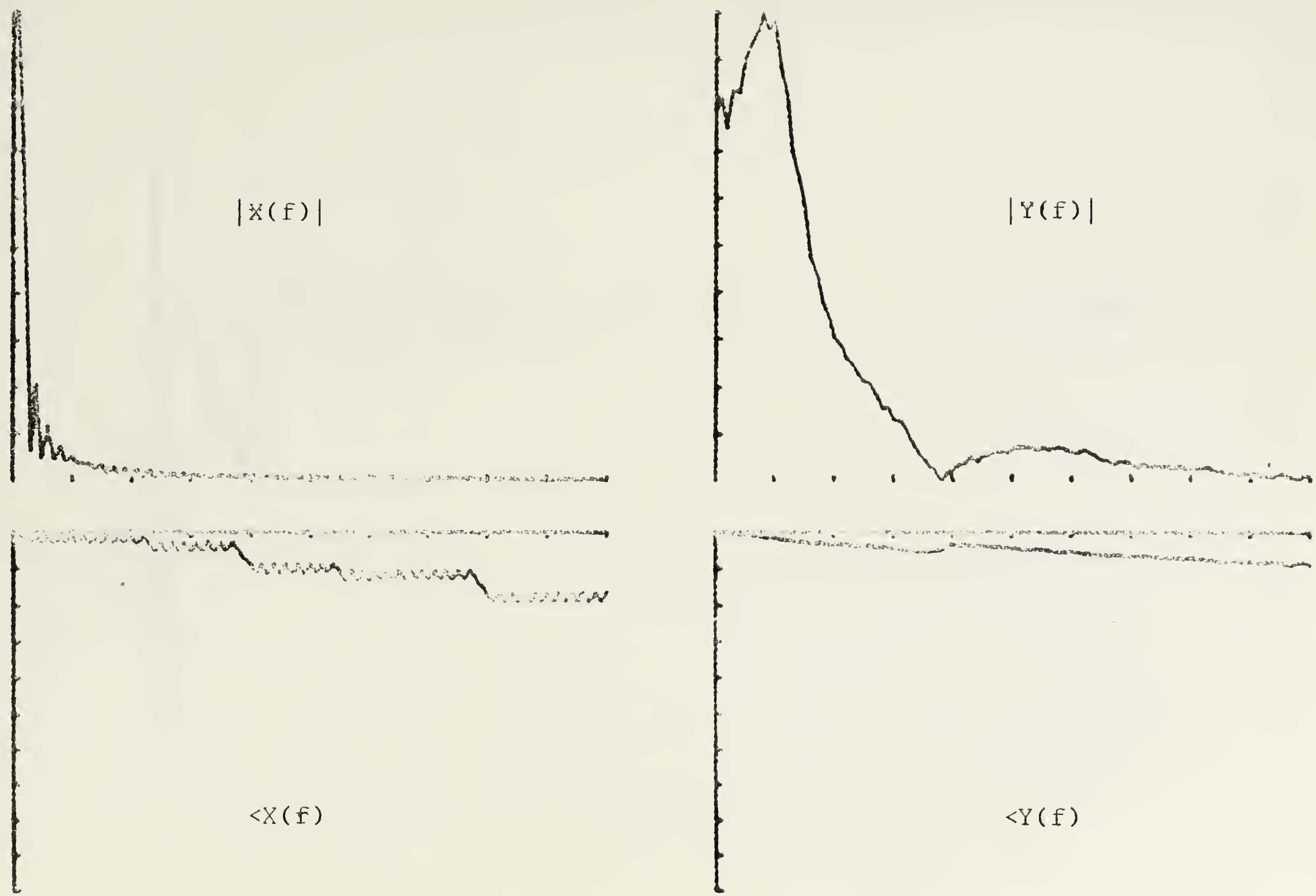

Figure 18.

IMPULSE RESPONSE OF ANTENNAS

Figure 19.

where $\bar{r}$ is the distance of an observer from the antenna, $\bar{J}s(\bar{r}',\tau)$ is the surface current density on the antenna at a distance $\bar{r}'$ from the origin, and τ is the propagation delay time, such that $\tau=t-r/c$. From equation (27) and (28), the far-zone fields radiated are proportional to the time derivative of the surface current density on the antenna. Intuitively, this implies that the transmitting antenna functions as a differentiator with respect to an input incident signal. The far-zone field response to a step input driving voltage will be impulse shaped. Similarly, if an impulse driving voltage was inputted, the far-zone field response would be the derivative of an impulse or a doublet function. This is the result that would be anticipated for the impulse response of the transmitting antenna. The experimental response bears this supposition out in that it resembles a smoothed doublet function as shown in Figure 19. In addition to this, the experimentally determined impulse response can be shown to be valid by comparison with Figure 13, which is the impulse response of the one meter wire monopole antenna and the TEM horn. In this comparison, both curves are identical for the first four nanoseconds of each response. After this time period, reflections from the end of the one meter, monopole antenna make the impulse responses differ. In Figure 19, the transmitting antenna was long enough so that reflections from the end of the antenna were time windowed out by the oscilloscope; hence,

the impulse response contains no reflections. Since the step response of the one meter wire antenna was proved to be valid, the impulse response of the one meter antenna is likewise correct. From this inference, a comparison of the similarities in Figures 13 and 19 make the impulse response of the transmitting antenna a valid representation for the first four nanoseconds of time.

There are several constraints imposed by the TEM horn antenna which may cause Figure 19 to differ from its actual value. The first limitation is due to the TEM horn antenna not being in the far-zone field of the transmitting antenna; and the second, which is a consequence of the first, is that the flare angle of the TEM horn is not wide enough for the horn to receive the electromagnetic fields at its aperture when the fields are radiated by the upper portions of the transmitting antenna. A third constraint is based on the assumption that a TEM wavefront exists at the aperture. This is valid only as long as the wavelengths of the received signal are large compared to the TEM horn aperture dimensions. There is a possibility that higher frequencies may be distorted or attenuated while propagating through the horn antenna. This would account for smoothing which may occur in the measured scattered response from a target on the image plane.

C. SIGNAL PROCESSING SCHEME

A significant problem in signal processing schemes is the estimation of signal parameters such as the mean, root mean square, and variance in the presence of noise. The noise, which appears in the measurements made in the scattering laboratory, is generated by external and internal sources. The broadband receiving characteristics of the TEM horn antenna make the system especially susceptible to both man-made and natural external noise sources. Man-made sources include television, radio, and radar emissions from the local area. Natural external sources, dependent on atmospheric conditions, change throughout the day. Thermal agitation of electrons is increased during mornings and afternoons when the antennas and the image plane are directly exposed to the sun. Conversely, thermal excitation of electrons is reduced at night when moisture condenses on the image plane and cooling of surface temperatures results.

Internal noise has several sources within the system. Mutual interactions between the transmitting and receiving antennas, as well as the interaction between the antennas and a target, produce invalid signal responses unless sufficient separation is maintained. To minimize antenna interactions, the TEM horn antenna was placed approximately three meters from the transmitting antenna. With power reduction inversely proportional to the square of the

distance between the antennas, the interactions are reduced by a factor of about 10 as compared to a separation of one meter or less between the antennas used in the prototype models. Separation between the antennas and a target is dependent on the aspect angle of the target to be viewed. When placing the target on the image plane, it should be positioned as far away from the antennas as possible while still receiving a target response of sufficient amplitude. In this way the measurement of far-field scattering quantities is optimally approximated.

The antenna responses also include pollution by internal noise sources. Multimode propagation, edge diffraction, and fringing fields cause distortion and dispersion of the received signal which alter the TEM wavefront at the aperature of the horn antenna.

Another significant internal noise source in the system is the pulse generator. Johnson noise, caused by circuit components in the pulse generator, is always present. Another problem is created when the pulse generator is interfaced with the digital processing oscilloscope. When the computer program subtracts the incident averaged waveform from the augmented averaged waveform, there is sometimes a shift between the two signals on the horizontal time axis. This shift produces a noise spike in the resulting target response. The amplitude of this spike is random, but the spike occurs at the same points in time

as the leading and falling edges of the incident signal. These noise spikes introduce erroneous high frequency components in the spectrum and thus invalidate the results. To illustrate this phenomenon, a set of fifty signals was measured and averaged. Without changing any settings on the oscilloscope or the pulse generator, another set of fifty signals was measured and averaged. The two averaged signals are shown in Figure 20. The difference between the two waveforms is shown in Figure 21. The amplitudes of the noise spikes are significantly greater than the other noise present in the system. Signal averaging does not decrease the noise spike. Increasing the number of signals to be averaged increases the time to measure a set of waveforms. This often causes the shift on the time axis to drift further, resulting in an even larger noise spike. Since the amplitude of the spike is random, better results can be usually obtained by repeating the complete set of measurements.

In addition to the waveforms displayed in Figures 20 and 21, the peak values, root mean square and mean values are also given. Even though the incident and augmented waveforms in Figure 20 are two sets of waveforms from the same ensemble, the values of the statistical parameters differ to some degree. In order to make the estimate of the mean an accurate approximation of the true mean, ensemble waveform averaging is used to reduce noise in the

Figure 20. WAVEFORM STATISTICS

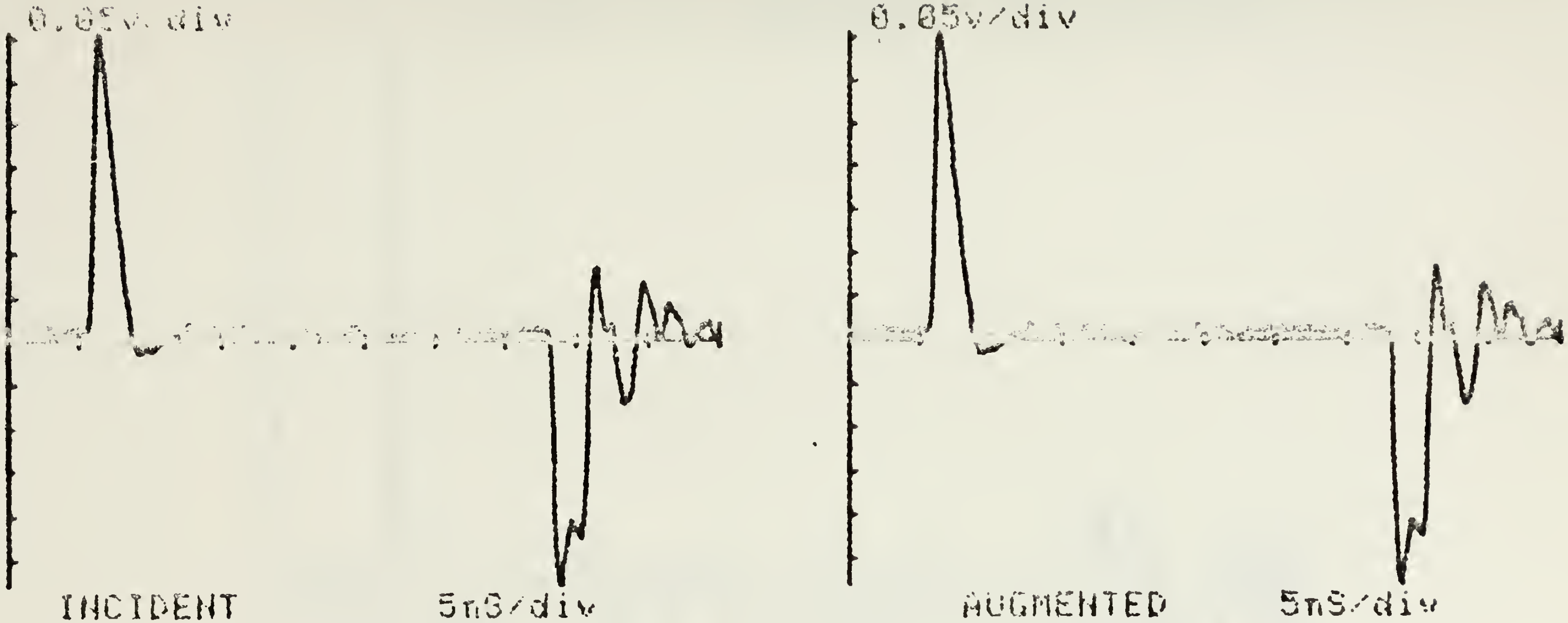

FOR N= 50

	INCIDENT	AUGMENTED
MAXIMUM PEAK VALUE (VOLTS)	0.3569	0.3557
MINIMUM VALUE (VOLTS)	0.2795	-0.2802
RMS VALUE (VOLTS)	0.0749	0.0747
MEAN VALUE (VOLTS)	0.0106	0.0095

Figure 21. Difference of Two Identical Waveforms

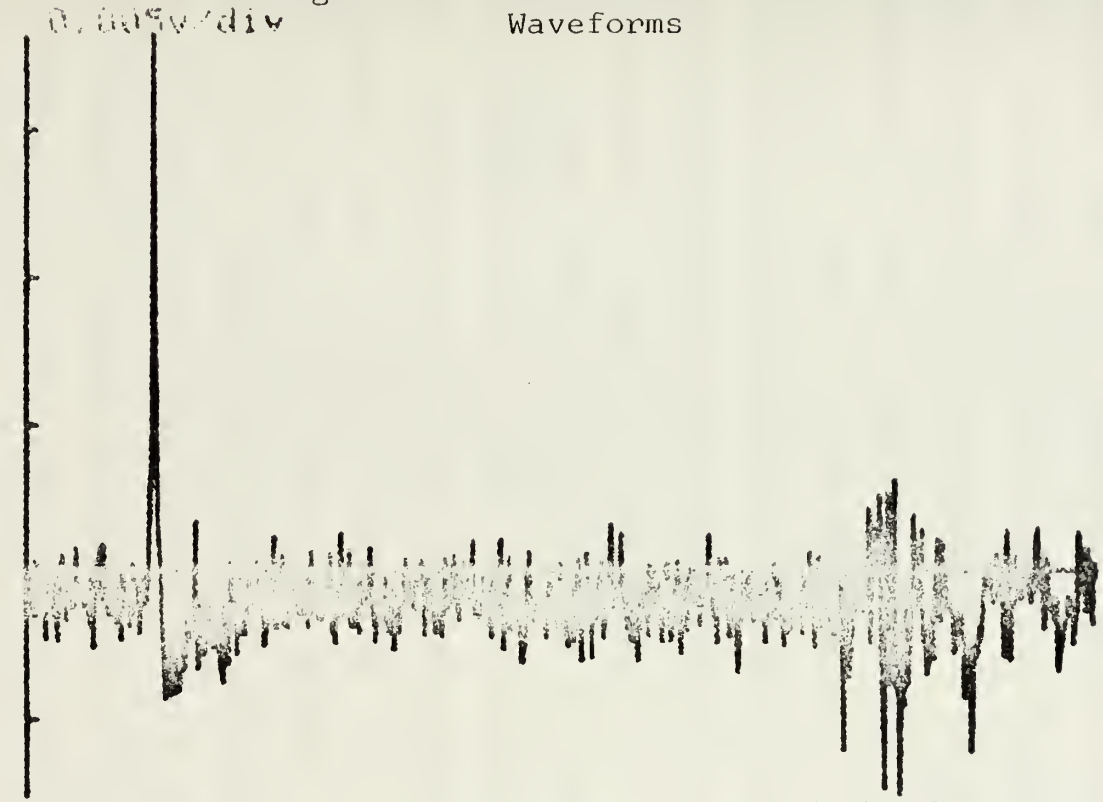

MAXIMUM PEAK VALUE (VOLTS)	0.0133
MINIMUM VALUE (VOLTS)	-0.0076
RMS VALUE (VOLTS)	0.0019
MEAN VALUE (VOLTS)	-0.0011

system. To determine the effectiveness of waveform averaging, the following tests were made. First, the pulse generator was disconnected from the coaxial cable leading to the transmitting antenna. In place of the pulse generator, a matched 50 ohm load termination was connected to the cable. The image plane was cleared of targets, and the pulse generator was used only to trigger the oscilloscope. By measuring the received signals with the TEM horn antenna, the amount of noise in the system could be determined. If an incident noise waveform and augmented noise waveform were both measured and then subtracted, the resulting noise is what could be expected to be present in the target response. Three different values of N, the number of waveforms to be averaged, were selected; these were N=1, N=10, and N=50. Figures 22 and 23 show the noise present for N=1 and N=50 cases. The following chart shows the effect that increasing N has on noise reduction for the target response. These results compare very favorably with the theoretical reduction of the root mean square value by the square root of N produced by ensemble averaging of random variables. It was determined that N=50 reduced the noise to an acceptable level.

Figure 22. TARGET RESPONSE

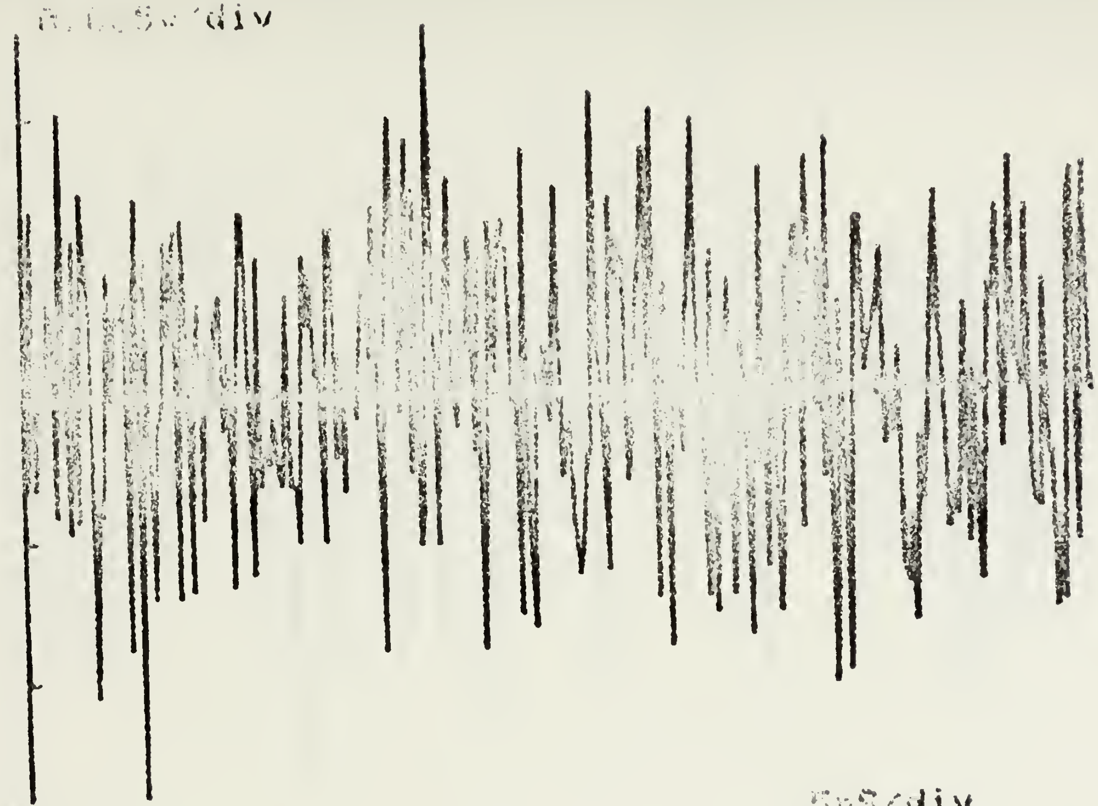

FOR N= 1

MAXIMUM PEAK VALUE (VOLTS)	0.0131
MINIMUM VALUE (VOLTS)	-0.0141
RMS VALUE (VOLTS)	0.0035
MEAN VALUE (VOLTS)	0.0032

Figure 23. TARGET RESPONSE

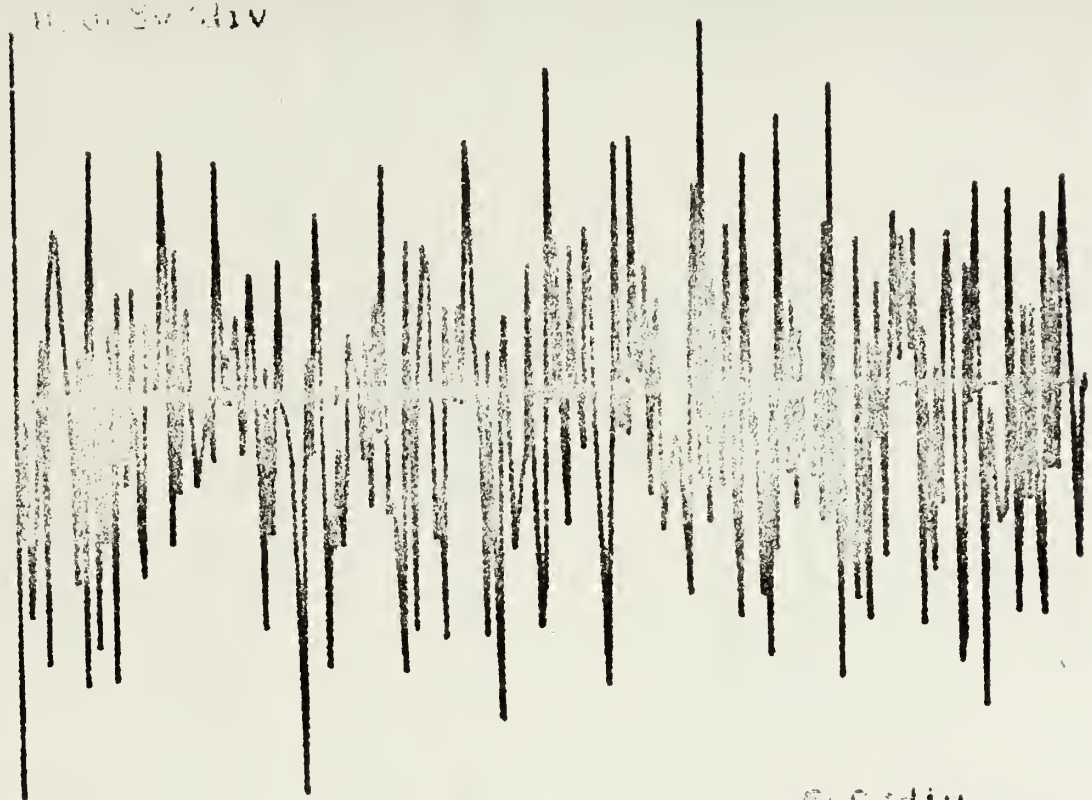

FOR N= 50

MAXIMUM PEAK VALUE (VOLTS)	0.0017
MINIMUM VALUE (VOLTS)	-0.0019
RMS VALUE (VOLTS)	0.0005
MEAN VALUE (VOLTS)	0.0000

	N=1	N=10	N=50
Maximum value (volts)	0.0131	0.0048	0.0017
Minimum value (volts)	-0.0141	-0.0041	-0.0019
Rms value (volts)	0.0035	0.0011	0.0005
Mean value (volts)	0.0002	0.0001	0.0000

In the computation of the statistical parameters, the estimate of the mean value $\hat{\bar{X}}$ is computed by

$$\hat{\bar{X}} = (1/512) \sum_{i=1}^{512} X(i) \tag{29}$$

where X(i) is the ith sample of the 512 samples made by the digital processing oscilloscope. Use of equation (29) assumes ergodicity, that is a time average is equivalent to the ensemble average of the waveforms.

The estimate of the root mean square value $\hat{X}(RMS)$ is given by

$$\hat{X}(RMS) = \sqrt{(1/512) \sum_{i=1}^{512} [X(i)]^2} \tag{30}$$

An estimate of the variance is not computed in the program but is easily determined from the statistical parameters already computed. The estimate of the variance $\hat{Var}(X)$ is determined by

$$\hat{Var}(X) = (1/511) \sum_{i=1}^{512} [X(i) - \hat{\bar{X}}]^2 \tag{31}$$

where the value of 511 or N-1 is an unbiased estimator.

D. DATA PROCESSING HARDWARE

1. Digital Processing Oscilloscope

The digital processing oscilloscope (DPO) used in the scattering range is arranged to make sampling measurements of fast waveforms. In addition to this, the DPO is capable of storing four waveforms in an integral memory and is also a computer compatible oscilloscope which provides an interface to the system minicomputer.

The digital processor unit of the DPO consists of six sections and an asynchronous bus. The system bus operates on a first-come, first-served basis and provides all sections of the processor with parallel access to power, address lines, control lines, and data lines. Figure 24 shows a block diagram of the processor unit.

Incoming signals to the DPO are received by the acquisition unit of the oscilloscope. Signal flow between the CRT display, the acquisition unit, and the processor is then handled by the signal interface unit. Signal sampling for the processor is done by the sample and hold section. Horizontal and vertical samples are made every 6.5 microseconds regardless of oscilloscope sweep speed. For sweeps

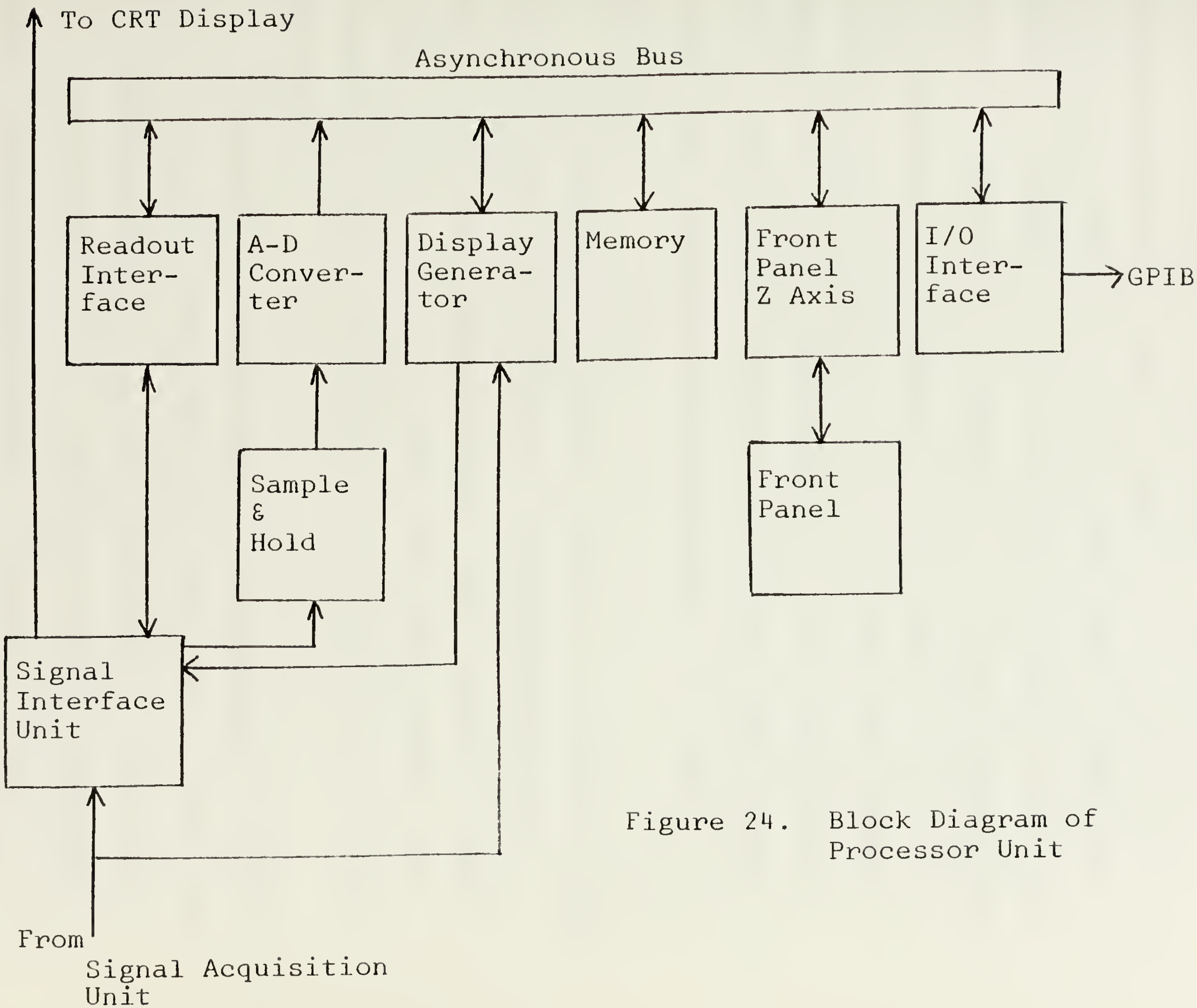

Figure 24. Block Diagram of Processor Unit

slower than 0.5 milliseconds/division, all 512 horizontal sample points are filled in a single sweep. When repetitive waveforms are sampled at sweep speeds faster than 0.5 milliseconds/division, updated samples are continuously provided while the DPO is in the STORE mode. When the processor is placed in the HOLD mode, a complete waveform is held in memory and is composed of old and new samples. For non-repetitive waveforms at sweep speeds faster than 0.5 milliseconds/division not all 512 horizontal memory locations are filled, and resolution of the waveform is reduced. Graphs are provided in the users manual which give the time required to fill the memory for various sweep speeds.

Conversion of the analog signal to a digital signal compatible with memory storage is accomplished by the analog to digital (A-D) converter. The horizontal sample is converted to a nine bit word (2**9 =512 points), and the vertical sample is converted to a ten bit word (2**10 = 1024 points).

After the analog signals are digitized, the memory section stores the waveforms as 512 horizontal points with 1024 possible levels of vertical resolution at each point. Each of the 512 horizontal locations contains sequential samples which are single-valued. The memory consists of 4096 words partitioned into eight distinct divisions of 512 words each. Four divisions are reserved for the storage

of waveforms. Each of the four divisions has four fields associated with it. These fields are used for the storage of waveform information such as scale factor data or mini-computer generated messages. Information stored in the four fields can be displayed simultaneously with the waveform on the CRT display.

The display generator of the processor unit is used to display waveform data on the CRT which has been placed in memory by the A-D converter or the minicomputer. Two modes of CRT display are possible, an X-Y mode or a Y-Time mode. Only the Y-Time mode is compatible with memory storage. When a sampled waveform is displayed, the display generator uses a linear interpolation feature to connect all adjacent points with line segments.

Finally, the Input/Output interface section of the processor acts as a bilateral link between the processor and minicomputer; the front panel section allows operation of the DPO from the front panel; and the readout interface converts readout information from the acquisition unit into ASCII code for storage in memory and reconverts it into readout information for the display unit.

2. Minicomputer

Control of data acquisition and signal processing is managed by a 64k minicomputer system controller. Figure 25 presents a block diagram of the controller hardware

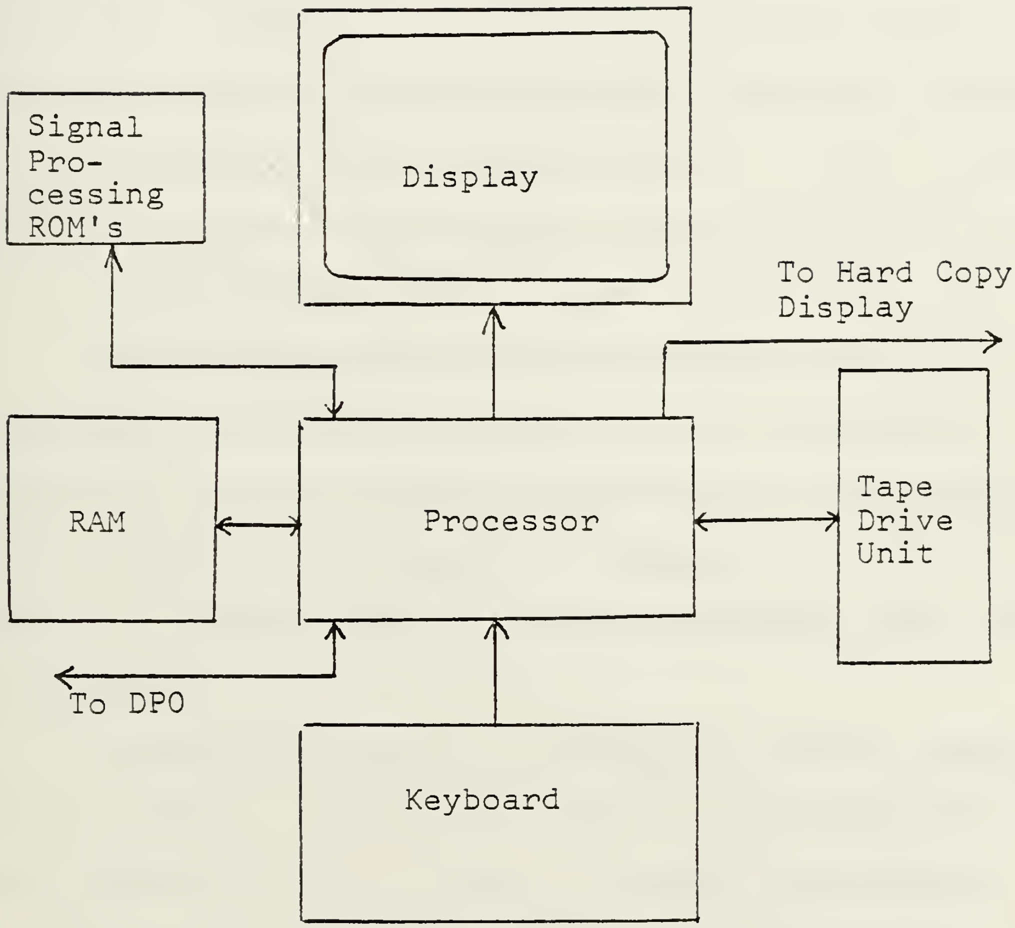

Figure 25. Block Diagram of System Controller Hardware

which is interfaced with the DPO and a hard copy display unit. The keyboard is the primary input device for the system. Each time a key is pressed an ASCII coded representation is written into a random access memory (RAM) location called a line buffer and displayed on the CRT. When the return key is pressed, the contents of the line buffer is written into memory by the minicomputer processor provided the input conforms to the proper syntax. If not, the message is displayed again on the CRT for editing along with a syntax error cursor indicating the location of the error.

The two magnetic tape units each provide 300k bytes of additional data storage capability for the system. The information storage is permanent and may be a software program or data to be processed by a program. All data flow between the magnetic tape unit and the RAM must pass through the processor.

The RAM provides 56k of temporary storage memory for keyboard entries, program instruction, and intermediate processing results. The contents of the RAM are destroyed when written over or power is removed from the system.

The system processor is the routing and computing device for the minicomputer. The processor directs all system operations, decodes program instructions, and performs arithmetic and logic operations. An integral part of the processor is the firmware permanently fixed in the system which interprets program instructions for processing. This

is known as the BASIC interpreter. Also, added are three signal processing read only memory (ROM) packs of up to 16k bytes of specialized programs. These ROM packs perform such operations as fast Fourier transforms (FFT), inverse fourier transforms (IFT), convolution, correlation, and high level text editing operations. The programming language used by the processor is Beginner's All-Purpose Symbolic Instruction Code (BASIC) developed in the nineteen sixties at Dartmouth College. Extensions of this language are incorporated for graphics displays and for transfer of data between internal and external devices.

The graphic system display is a cathode ray tube storage device which allows for interaction between the processor and the operator through the keyboard. The display screen retains the written image for viewing and hard copy reproduction. The addressable points on the CRT are defined in terms of graphic display units (GDU). There are 130 horizontal addressable GDU's and 100 vertical addressable GDU's.

The general purpose interface bus (GPIB) links all peripheral devices to the system. GPIB specifications conform to IEEE standard 488-1975. The transfer mode between devices is byte-serial, bit-parallel. External devices are serviced by interrupt instructions. Enable, polling and data transfer commands are available under program control.

E. SOFTWARE DEVELOPMENT

The following logic flow diagram presents an overview of the software program developed to perform all signal processing necessary from the initial acquisition of a signal from the receiving antenna on the image plane to a graphical display of the impulse response of a target. Appendix A contains the software program

Figure 26. Logic Flow Diagram

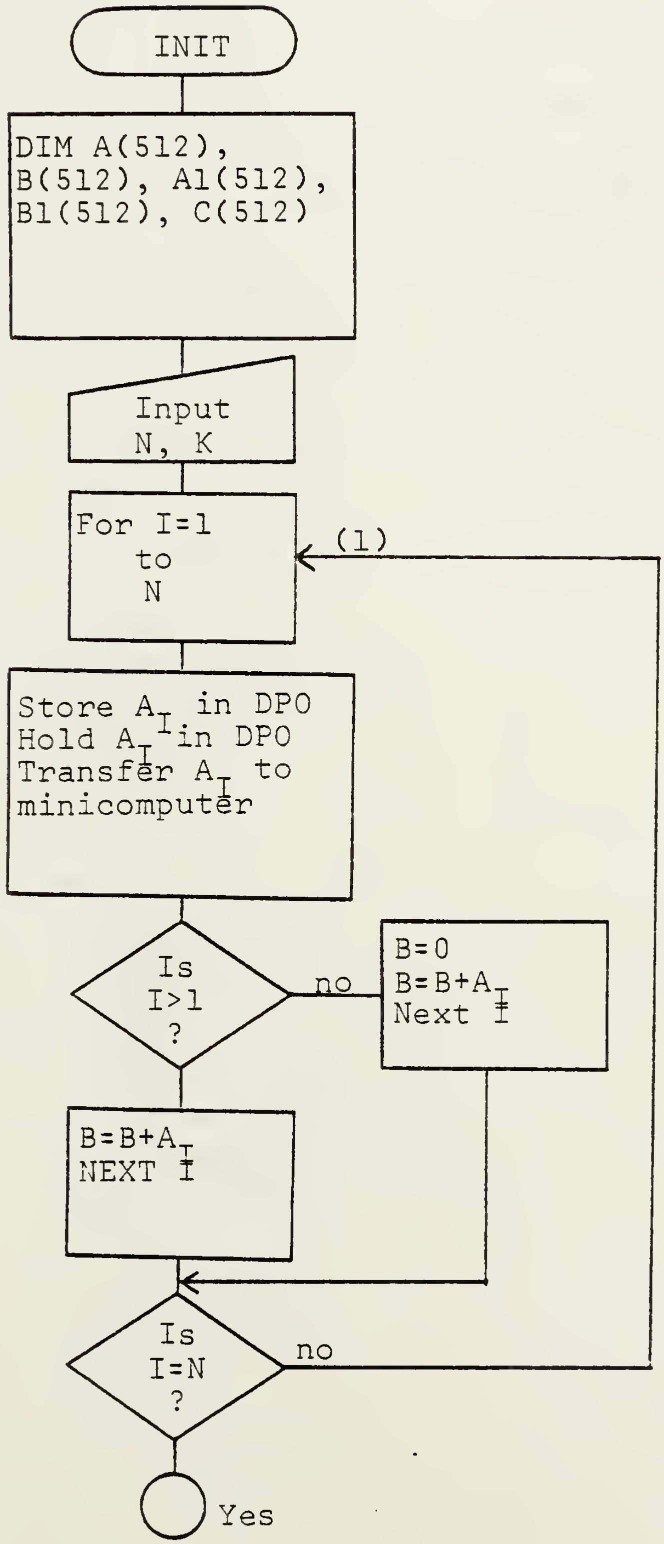

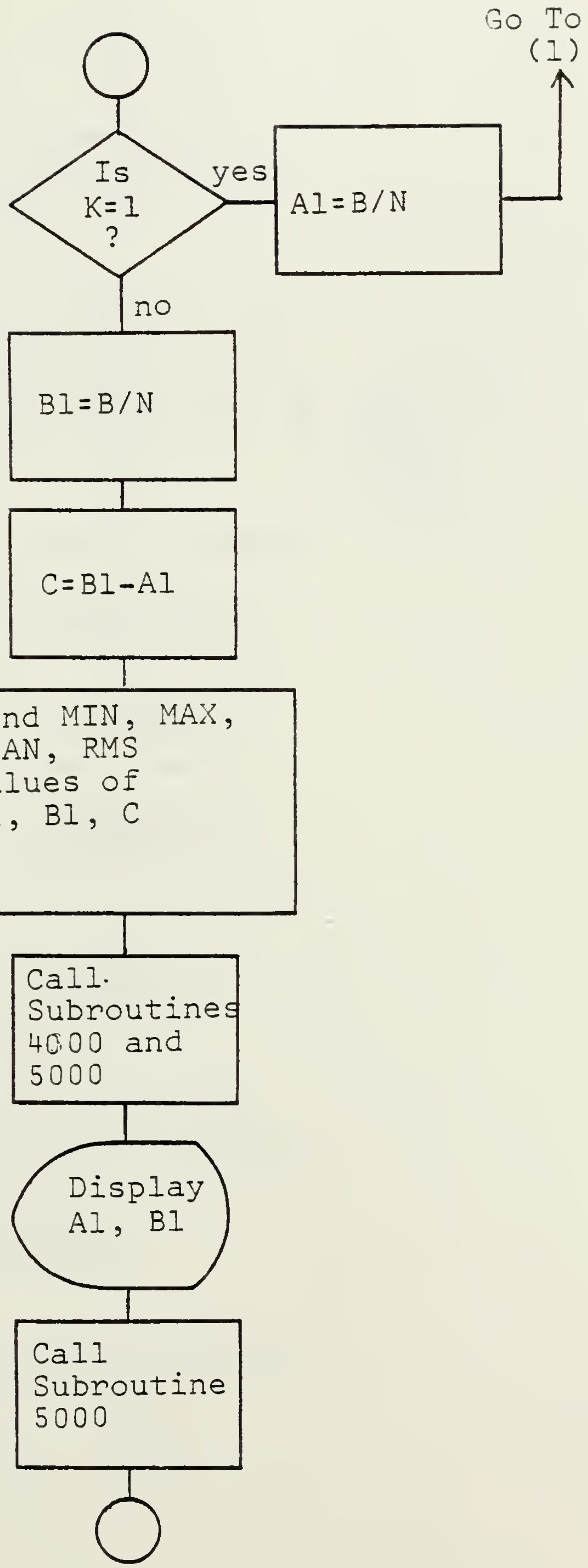
Go To
(1)
Is
K=1
?
yes
A1=B/N
no
B1=B/N
C=B1-A1
Find MIN, MAX,
MEAN, RMS
Values of
A1, B1, C
Call
Subroutines
4000 and
5000
Display
A1, B1
Call
Subroutine
5000

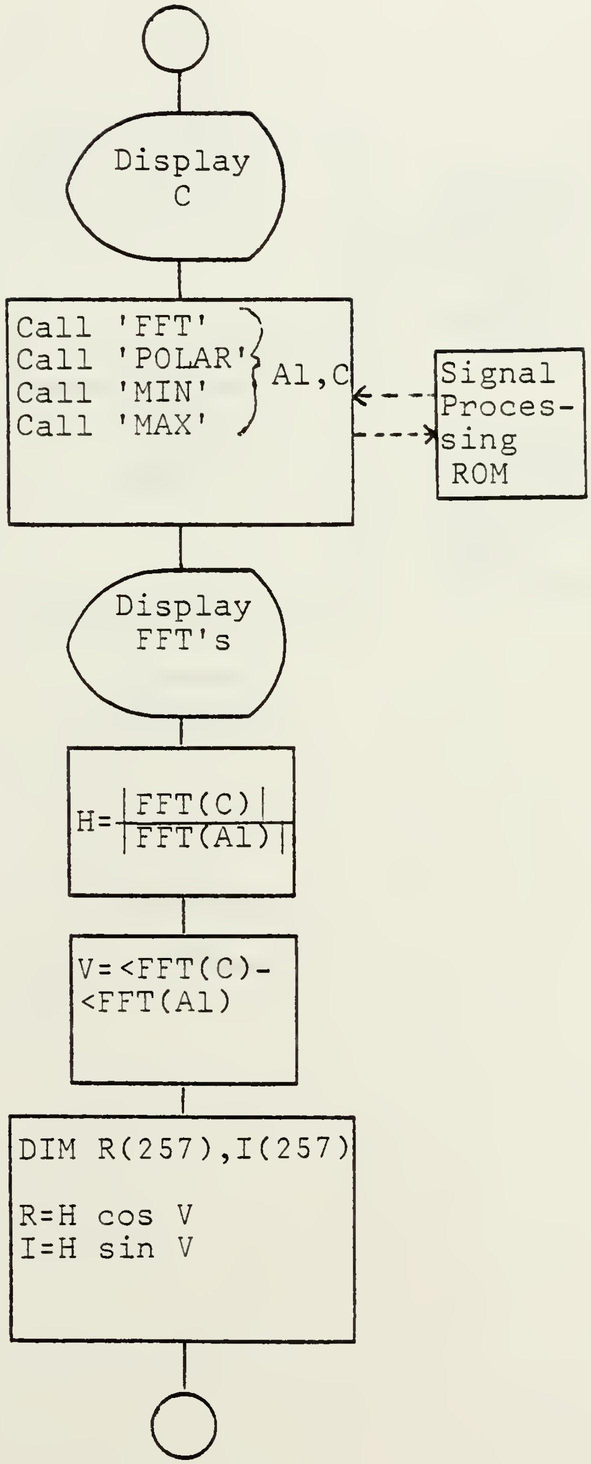
Display C
Call 'FFT'
Call 'POLAR'
Call 'MIN'
Call 'MAX'
A1,C
Signal Proces-sing ROM
Display FFT's
H=|FFT(C)| / |FFT(A1)|
V=<FFT(C)-<FFT(A1)
DIM R(257),I(257)
R=H cos V
I=H sin V

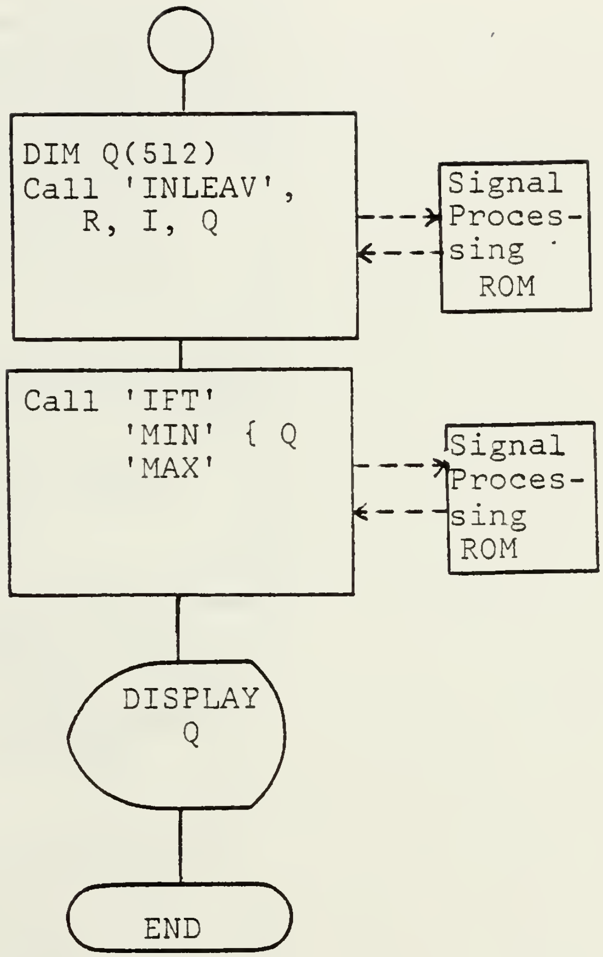
DIM Q(512)
Call 'INLEAV',
R, I, Q
Signal Processing ROM
Call 'IFT'
'MIN' { Q
'MAX'
Signal Processing ROM
DISPLAY
Q
END

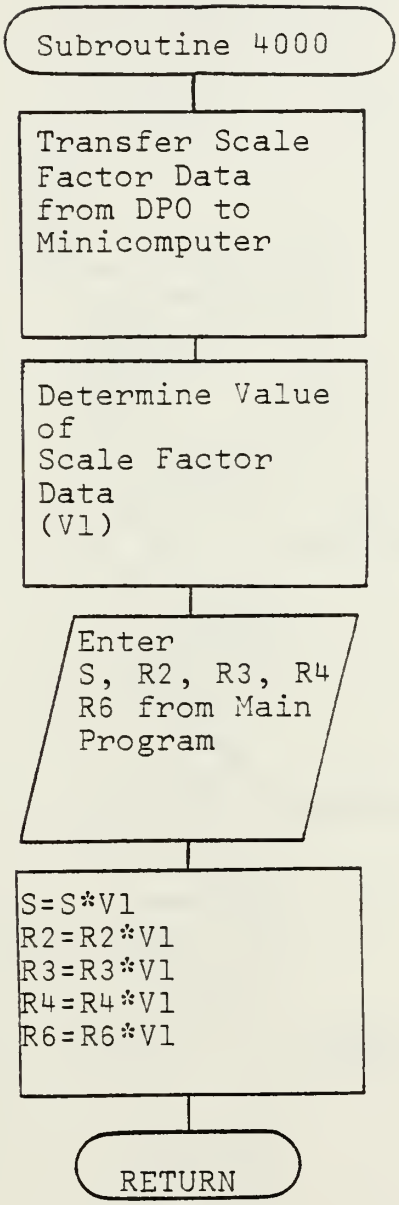
Subroutine 4000
Transfer Scale Factor Data from DPO to Minicomputer
Determine Value of Scale Factor Data (V1)
Enter S, R2, R3, R4 R6 from Main Program
S=S*V1
R2=R2*V1
R3=R3*V1
R4=R4*V1
R6=R6*V1
RETURN

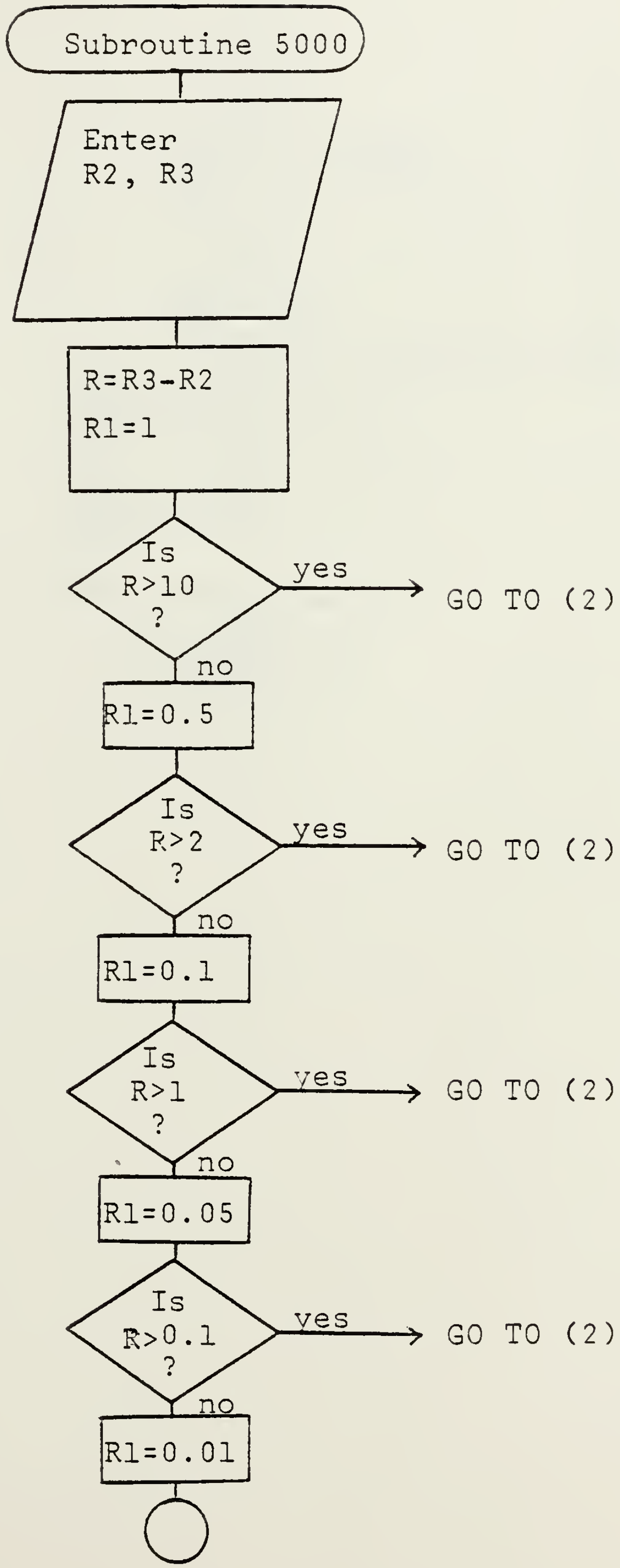
Subroutine 5000
Enter
R2, R3
R=R3-R2
R1=1
Is
R>10
?
yes
GO TO (2)
no
R1=0.5
Is
R>2
?
yes
GO TO (2)
no
R1=0.1
Is
R>1
?
yes
GO TO (2)
no
R1=0.05
Is
R>0.1
?
yes
GO TO (2)
no
R1=0.01

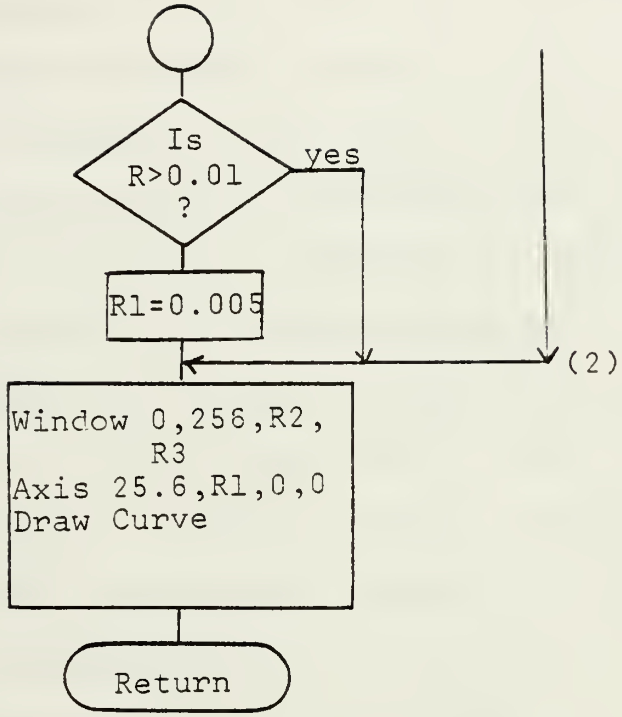
Is
R>0.01
?
yes
R1=0.005
(2)
Window 0,256,R2,
R3
Axis 25.6,R1,0,0
Draw Curve
Return

The program is designed to request N, the number of waveforms to be averaged, interactively from the operator through the minicomputer keyboard. After the value of N has been entered, the program returns that value for verification and asks the operator if the image plane is properly set up. After receiving an affirmative response of "YES" from the operator, the program determines if the signals to be averaged will contain a target response (augmented waveform) or if the range will be clear of a target and only the direct response (incident waveform) will be measured. This requires the operator to enter a value K of "1" for incident waveform averaging or "2" for augmented waveform averaging. When this value K is entered, the program returns that value for verification. The operator then inputs the command "GO" and operation of the DPO is taken over by the minicomputer.

Lines 280-410 are a FOR/NEXT loop which instruct the DPO to store then hold a waveform in memory. Lines 310-315 from a BUSY/WAIT loop which slows the execution speed of the program to allow for waveform storage time. The minicomputer processor then prepares to transfer the digitized waveform from the DPO memory to the minicomputer

memory. After the interface bus is clear, the transfer is made on command. Once the waveform is in the mini-computer memory, the process is repeated until N waveforms have been acquired. Each time a waveform is transferred from the DPO , it is added to the sum of the previous waveforms until the resultant matrix of time-sampled values B is obtained where

$$B = \sum_{i=1}^{N} A_i \tag{32}$$

For incident waveforms the ensemble averaged time-sampling matrix A1 is determined where

$$A1 = B/N \tag{33}$$

For augmented waveforms the ensemble averaged time-sampling matrix B1 is computed such that

$$B1 = B/N \tag{34}$$

The program determines next if all signal averaging is complete. If not, the value of K is changed and the program branches back to the FOR/NEXT loop to process another set of waveforms. When the averaging is complete, the incident waveform is subtracted from the augmented waveform such that

$$C = B1-A1 \tag{35}$$

Lines 700-940 calculate the maximum and minimum values, mean values, and root mean square values of waveforms C, B1, and A1. The maximum and minimum values are used for plotting purposes in the program to determine the vertical window length of the graphical displays.

The first graphical results present the incident and augmented averaged waveforms along with the peak values, mean and rms values of B1 and A1. Refer to Figure 27 for an example of this graphical format. Two subroutines are used to scale the sampled waveform data and to graphically plot the waveforms.

Before subroutine 4000 is called, each of the 512 horizontal points has some discrete value between 0 and 1024. Subroutine 4000 transfers the voltage scale factor and the time scale factor from field (F0) commencing at address 2048 of waveform A in the DPO to the minicomputer processor. The sampled data values are then multipled by the appropriate scale factors.

Subroutine 5000 determines the scale factor of the ordinate of each graph based on the maximum and minimum values previously determined then plots a smooth curve for each waveform. In a similar manner the target response C is scaled, then plotted using subroutine 5000. This graph is followed by the maximum, minimum, mean and rms values of the target response. Figure 28 provides an example.

The target response C represents the convolved tansient responses of the transmitting and receiving antennas convolved along with the transient response of the target. In order to isolate the transient target response, additional signal processing is necessary. First, the fast Fourier transform (FFT) of waveforms C and A1 are computed with the use of one of the signal processing ROM's. The FFT command performs a fast calculation of the discrete Fourier transform (DFT) given by

$$C(k) = \sum_{n=0}^{511} c(n)e^{-j2\pi nk/572} \quad k=0,1,2,....255 \qquad (36)$$

where C(k) is the kth Fourier coefficient and c(n) refers to the (n+1)th element of the real sampled data of waveform C. A similar set of values is generated for waveform A1. In this particular FFT algorithm, C(1) and A1(1) represent the direct current value of those signals. C(2) and A1(2) represent the value of the FFT at the Nyquist frequency which is one-half the sampling frequency. The remaining values C(3)-C(511) and A1(3)-A1(511) represent the interleaved real and imaginary terms for the Fourier coefficients.

The "POLAR" command allows for easier interpretation of the FFT results by converting the rectangular Fourier coefficients into polar form where array components are expressed in terms of magnitude and phase angle. Lines 1930-2240 generate graphical displays of magnitudes and

phases of the FFT's of waveforms C and A1. See Figure 30. Since the time domain waveforms are real, the FFT's will be even and symmetric about the vertical axis; thus only 256 points are required for the magnitude of the FFT and 256 points for the phase of the FFT.

At this point the FFT of waveform A1 is the product of the system transfer functions of the transmitting and receiving antennas such that

$$A1(k) = H(k)\ Sr(k) \qquad k=0,1,\ldots\ldots 255 \tag{37}$$

where H(k) is the kth component of the transfer function of the transmitting antenna and Sr(k) is the kth component of the transfer function of the receiving antenna. The FFT of waveform C is the product of the transfer functions of the transmitting antenna, receiving antenna, and the target thus

$$C(k) = T(k)\ H(k)\ Sr(k) \qquad k=0,1,\ldots .255 \tag{38}$$

where T(k) is the kth component of the target transfer function. The isolate T(k), the magnitude of (38) is divided by the magnitude of (37) so that

$$|T(k)| = |C(k)|/|A1(k)| \qquad k=0,1,\ldots .255 \tag{39}$$

and the phase of Al(k) is subtracted from the phase of C(k) such that

$$\angle T(k) = \angle C(k) - \angle Al(k) \qquad k=0, \ldots\ldots 255 \qquad (40)$$

Having determined the magnitude and phase of T(k), it is a simple matter ot convert T(k) from polar form to rectangular form. This is done in lines 2340-2370 of the program. Finally, the inverse Fourier transform (IFT) of T(k) is calculated by

$$h_t(n) = (1/512) \sum_{k=0}^{512} T(k)\, e^{+j2\pi nk/512} \qquad n=0,1,..511 \qquad (41)$$

where $h_t(n)$ is the (n+1)th element of the sampled data impulse response of the target. $h_t(n)$ is plotted as a function of time by lines 2430-2540 in the program.

To evaluate the signal processing scheme of the program, an ideal, time domain step function described by

$$x(k) = \begin{cases} 1.0 & k=0,1,\ldots.100 \\ 0 & k=101,102\ldots511 \end{cases} \qquad (42)$$

was input into the program as the averaged incident, sampled data waveform; and the averaged augmented, sampled data waveform was input as

$$y(k) = \begin{cases} k & k=0,1,\ldots\ldots 100 \\ 200-k & k=101,102,\ldots\ldots 200 \\ 0 & k-201,202,\ldots\ldots.511 \end{cases} \qquad (43)$$

See Figure 28. When the program was executed, the target response was given as a triangular waveform shown in Figure 29. This is analogous to imputting a square wave into an unknown linear system obtaining the response as shown in Figure 27.

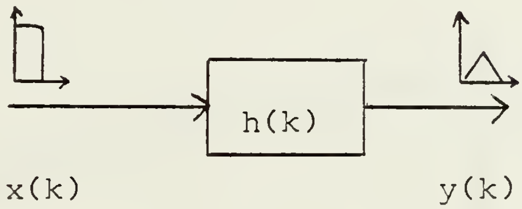

Figure 27

y(k) is expressed mathematically as the convolution of x(k) and h(k) such that

$$y(k) = x(k)*h(k) = \sum_{i=0}^{511} h(i)\, x(k-i) \quad \text{for } k-0,1,\ldots 511 \tag{44}$$

Since x(k) and y(k) are known, h(k), the system impulse response needs to be determined. This is precisely the main objective of the program.

Given y(k) and x(k), the FFT's of these functions are computed and displayed by the program as shown in Figure 30. X(nf), the nth component of the Fourier transform of x(k), has a $[\sin(2\pi nf)]/(2\pi nf)$ spectrum, and Y(nf), the nth

Figure 28. WAVEFORM STATISTICS

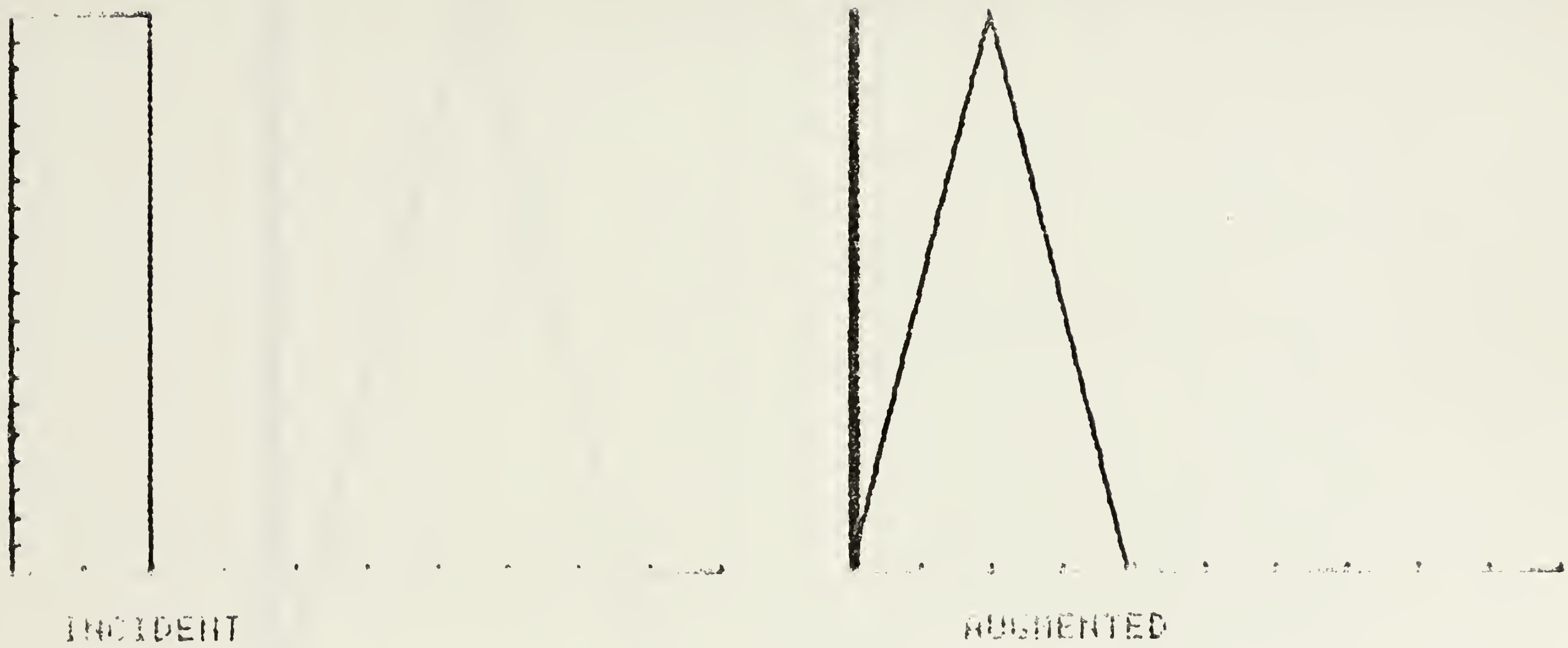

	INCIDENT	AUGMENTED
MAXIMUM PEAK VALUE (VOLTS)	1.0000	100.0000
MINIMUM VALUE (VOLTS)	0.0000	0.0000
RMS VALUE (VOLTS)	0.4419	36.0853
MEAN VALUE (VOLTS)	0.1953	19.5313

Figure 29. TARGET RESPONSE

MAXIMUM PEAK VALUE (VOLTS)	99.0000
MINIMUM VALUE (VOLTS)	0.0000
RMS VALUE (VOLTS)	35.6136
MEAN VALUE (VOLTS)	19.3359

Figure 30. FFT OF INCIDENT AND CONVOLUTED RESPONSES

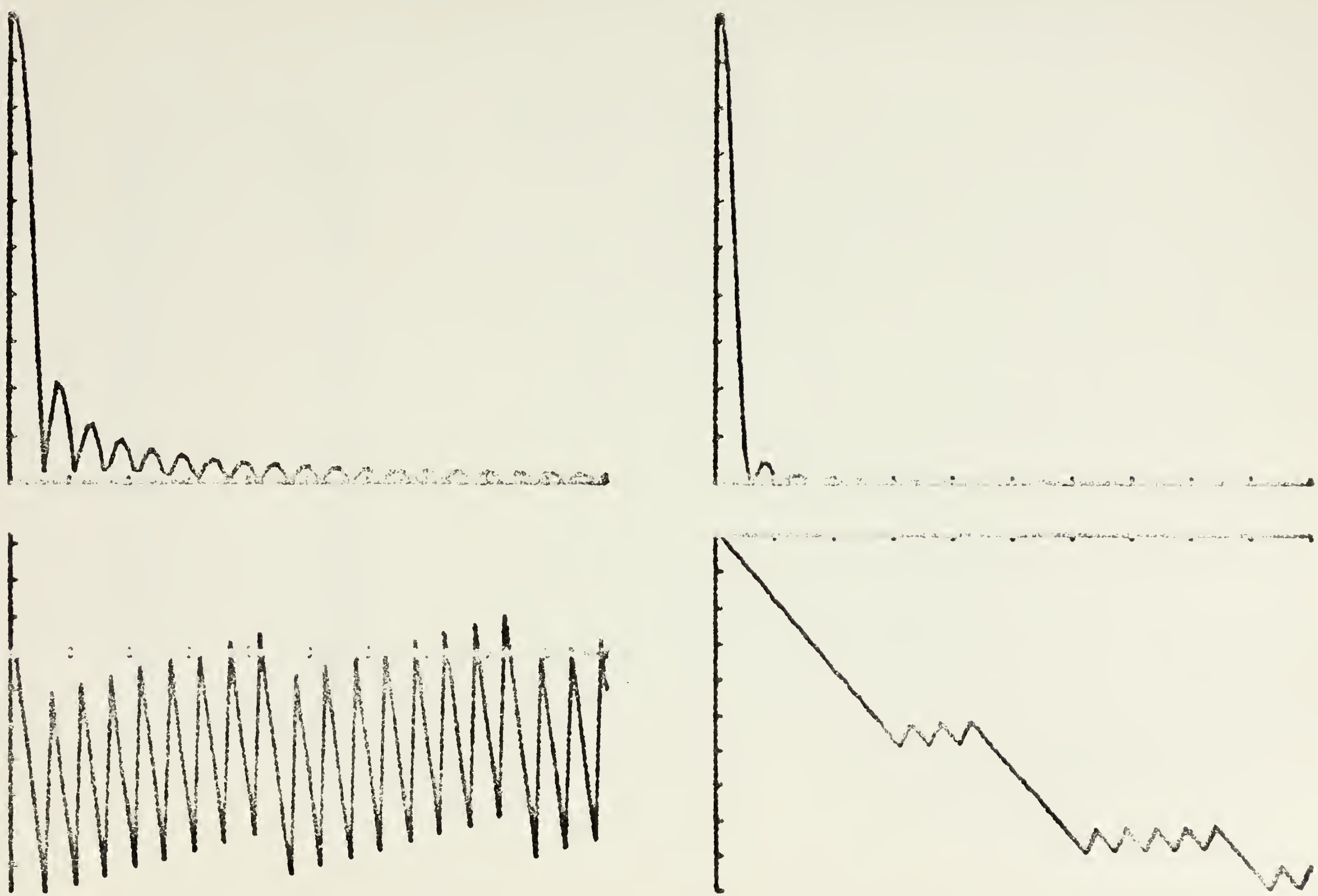

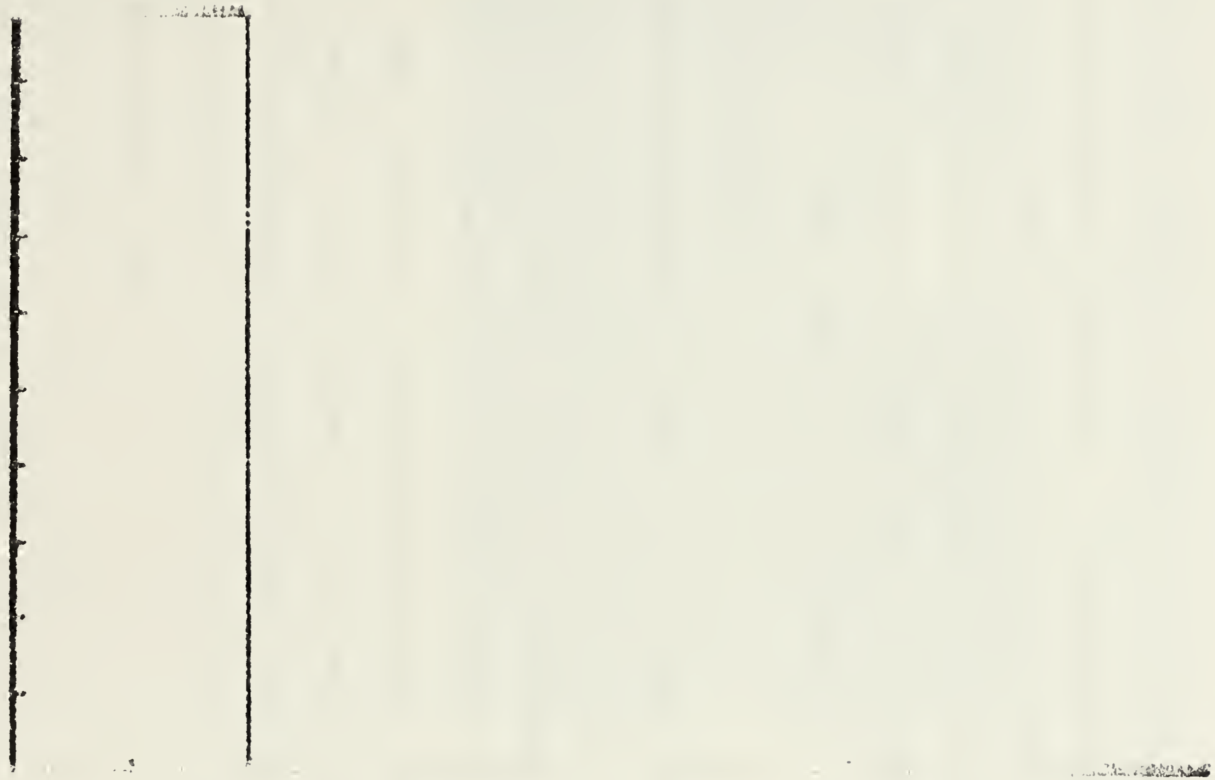

Figure 31. [illegible] OF TARGET

component of the Fourier transform of y(k), has a [sin(2 nf)/(2πnf)]**2 spectrum. H(nf) is then found by (39) and (40), and the resulting spectrum has a [sin(2πnf)]/(2πnf) shape.

After the IFT of H(nf) is computed, the impulse response is obtained and shown in Figure 31. This demonstrates the validity of the program in finding the impulse response of a system. By applying this same technique to the waveform signals obtained on the scattering range, the impulse response of a target on the image plane can be determined.

F. TARGET FABRICATION

The targets fabricated for use on the image plane consist of several axisymmetric configurations, where some are made of aluminum while others are made of plexiglas dielectric material. Figure 32 shows a sample of the target inventory. When placed on the scattering range, the targets are "mirror-imaged" by the surface of the image plane. In this manner a hemispherical target produces the scattered response of a sphere due to reflections from the conducting surface of the image plane.

Three basic designs, a cone, a cylinder, and a hemisphere, were machined from three inch diameter and six inch diameter aluminum stock. Later, some of the same designs were machined from a plexiglas material. Appendix B contains the specifications of the dielectric material. The dimensions

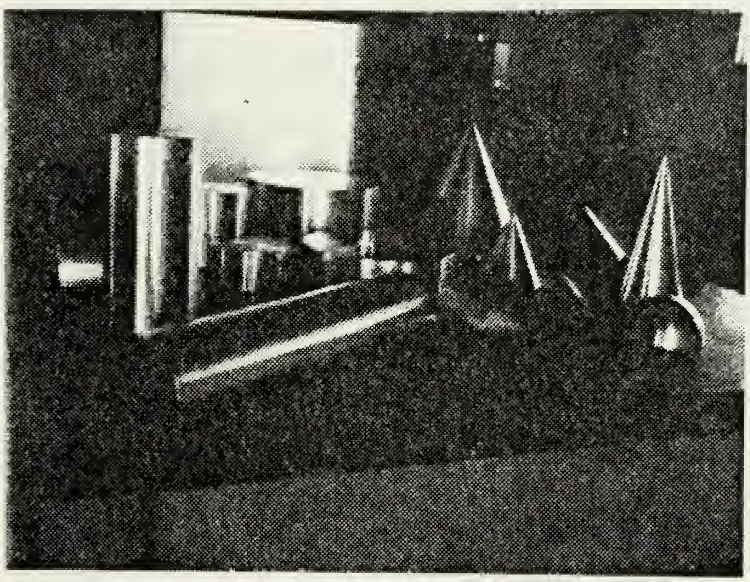

Figure 32. Sample of Representative Targets Used on the Image Plane

of the plexiglas targets were matched to those of the aluminum targets so comparisons between the conducting properties of the two materials could be made. In addition to these targets, a bisected version of the cylinder was fabricated to increase the number of aspect angles that this target could be viewed and to change the polarization of the incident fields. See the foreground of Figure 32. Several targets that were easy to fabricate have also been added to the inventory. These consist of two aluminum, rectangular plates and several metallic wires of different lengths.

Target resolution in scattering measurements is a problem dependent on the dimensions of the target. Several of the smaller targets, such as the three inch diameter hemisphere, have scattering responses which produce signal to noise ratios low enough to be indistinguishable from noise in the system regardless of their position on the image plane. Even signal averaging, used to reduce noise levels, is ineffective in enhancing the response.

In general, there is no rule of thumb on which to base the criteria for dimension designs. This is dependent on the type of scattering response produced by a target and on the noise present in the system. As an example, a wire has a damped sinusoidal target response, and usually can be detected by the DPO even with a length dimension slightly less than twelve inches. A target like the sphere, whose

time domain response is fast, is very difficult to detect. The three inch diameter sphere has never been detected on the image plane regardless of target position.

Solutions to this problem are addressed in Chapter IV, CONCLUSIONS AND RECOMMENDATIONS. In addition to the obvious solution of building larger targets, use of a higher voltage pulse generator, as planned, may improve target resolution. With a 1000 volt signal amplitude, 100 picosecond risetime, the scattered responses of the smaller targets may be increased enough to be identifiable. This remains to be tested.

III. SCATTERING LABORATORY MEASUREMENT RESULTS

Throughout much of the literature on time domain scattering as in references 14 and 15 for example, a regularization of an impulse is used as the incident waveform to illuminate targets. This incident field is referred to as a smoothed impulse and has the Gaussian form

$$E(t) = E_o e^{-a^2 \left(t-t_{max}\right)^2} \tag{45}$$

where E_o is the peak amplitude of the incident field, t_{max} is the time of peak amplitude or the signal mean, and a is a spread parameter related to the standard deviation σ of the Gaussian curve by

$$a^2 = \frac{1}{2\sigma^2} \tag{46}$$

This smoothed impulse is a convenient waveform because it has rapidly decaying time and frequency domain representations, and it is well-suited for numerical solution of the time domain scattering interaction.

If the incident field radiated from the transmitting antenna is approximated by this Gaussian waveform, the smoothed impulse response of a target can be measured by subtracting the incident waveform from the augmented waveform.

In this manner the "target response" determined by the software routine is the smoothed impulse response of a target. This result can then be compared to theoretical results in order to ascertain the validity of scattering range measurements.

A thin wire scatterer with a 50 cm length and a 0.161 cm diameter was selected as the target. The scattering properties of a wire are understood, and the numerical solution of its scattered fields is well-documented.

The experimental measurements were obtained as follows. Without the target on the image plane, 50 incident waveforms were sampled by the DPO and averaged by the minicomputer. The time-averaged incident waveform, shown in Figure 33a, is the approximation to the Gaussian waveform described by (45). The signal mean, t_{max}, is two nanoseconds, and the standard deviation, σ, is 0.75 nanoseconds.

To measure the augmented waveform, the target was placed directly between the transmitting and receiving antennas; a distance of 150 cm from the transmitting antenna, and a distance of 120 cm in front of the TEM horn antenna. 50 augmented waveforms were measured and averaged exactly as the incident waveforms were. The time-averaged, augmented waveform is shown in Figure 33b.

Figure 33. WAVEFORM STATISTICS

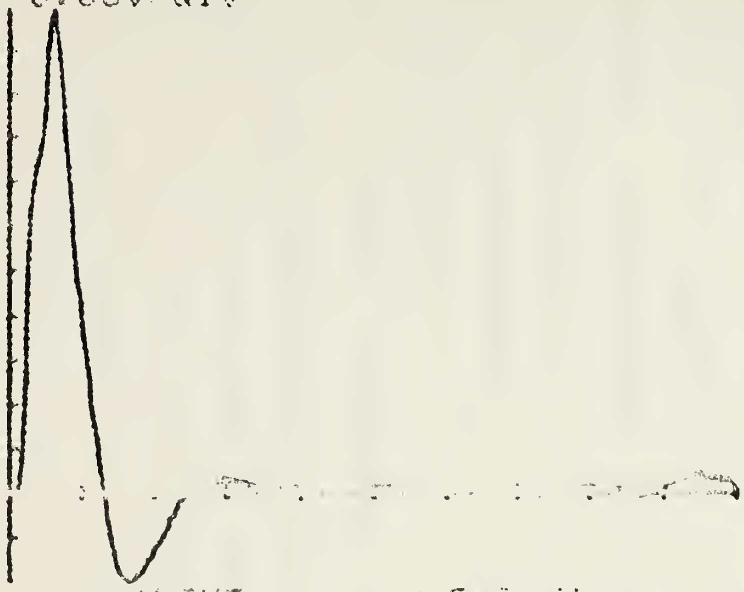

(a)

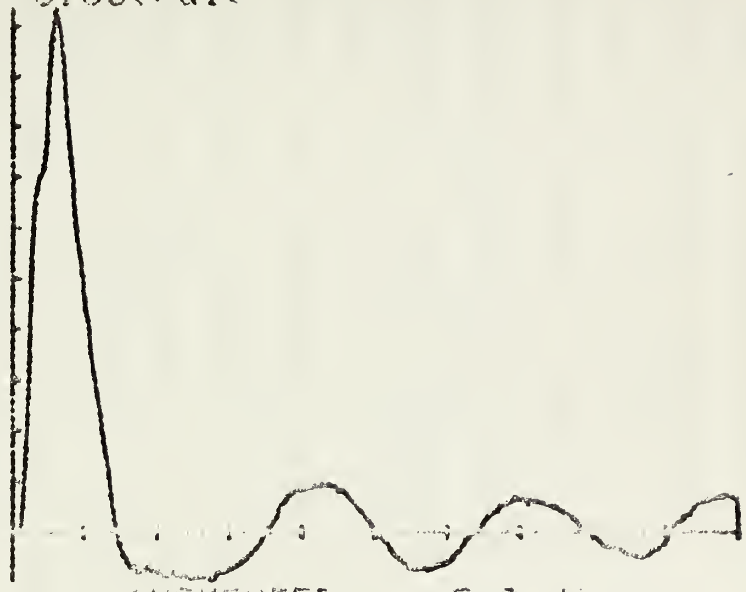

(b)

FOR N= 50

	INCIDENT	AUGMENTED
MAXIMUM PEAK VALUE (VOLTS)	0.5917	0.5232
MINIMUM VALUE (VOLTS)	-0.0938	-0.0466
RMS VALUE (VOLTS)	0.0868	0.0821
MEAN VALUE (VOLTS)	0.0169	0.170

When the incident waveform was subtracted from the augmented waveform, the smoothed impulse response for the wire scatterer was obtained. This measured voltage is presented in Figure 34, and is directly proportional to the scattered electric field from the target. Because of this relationship, a direct comparison between the measured voltage of the target response and the theoretical calculations of the scattered electric field can be made.

The method of moments described by Harrington in reference 16 is the basis for the numerical computation of the electric field scattered by the wire. In the computer program used, a 3.0 volt/meter electric field with Gaussian parameters of t_{max}=2.0 nanosec and σ=0.75 nanosec was broadside incident to the wire. The wire was divided into 22 segments for computational purposes. Scaling the theoretical values obtained by a factor of 0.002307 allowed the theoretical results to be plotted on the same coordinate axes as the experimentally determined values. Agreement between the two sets of data is seen to be excellent in Figure 34. Of the 18 theoretical values plotted, only one point deviated significantly from the measured data. This occurred at the first negative peak of the response. The deviation arises from the difference between the actual shape and the assumed Gaussian shape of the incident field on the wire.

Figure 34. TARGET RESPONSE

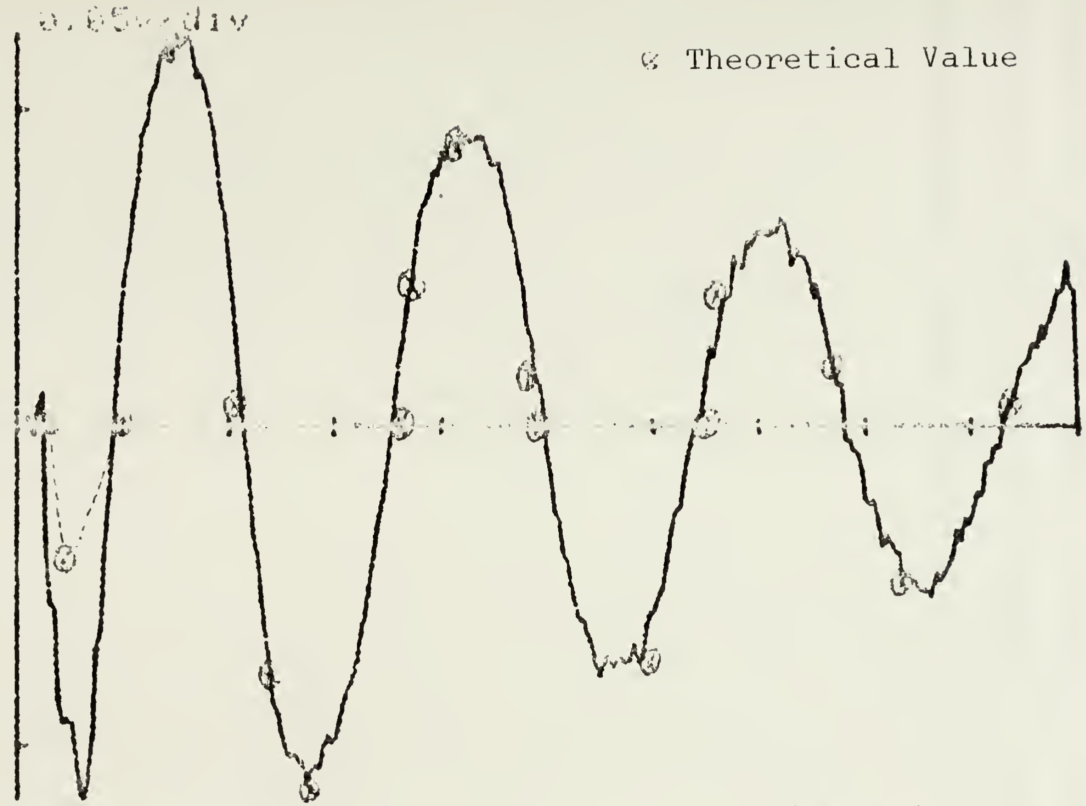

FOR N= 50

MAXIMUM PEAK VALUE (VOLTS)	0.0620
MINIMUM VALUE (VOLTS)	-0.0585
RMS VALUE (VOLTS)	0.0224
MEAN VALUE (VOLTS)	0.0001

The close correspondence between the theoretical and experimental data validates the measurements made in the scattering laboratory. However, further calibration of the scattering range is required to determine the amplitudes of the electromagnetic fields involved in scattering interactions. This will be necessary to develop target classification software routines in follow-on research.

IV. CONCLUSIONS AND RECOMMENDATIONS

The purpose in developing the time domain measurements scattering laboratory is to create a facility which will support research in the area of transient electromagnetics. Ultimately, this will assist in determining the feasibility of the design of advanced radar systems based on principles of time domain signal analysis. The work thus far completed has established a foundation in this area of research and has provided many opportunities for continued research in greater depth and on a broader basis. At the same time new problems have been created which must be addressed.

To summarize the accomplishments achieved since the project conception; there is now available a complete physical laboratory which contains the essential electronic hardware, antennas, and associated equipment, all properly interfaced, to make direct time domain measurements of the scattered electromagnetic fields from mirror imaged, symmetric objects. There exists software which is capable of managing the signal acquisition process of the electronic hardware, reducing the noise in the signal, extracting the smoothed impulse or gaussian pulse response of a target from the acquired signal; and finally, the software

is capable of storing and retrieving any necessary data or additional program instructions for further signal processing in 600 kilobytes of supplementary tape memory.

A. ANTENNAS

A problem that has arisen concerns the transmitting antenna. Above the image plane, a twenty-one foot wire, monopole antenna has been constructed to transmit the incident electromagnetic field. Its increased length over a previous antenna tested offers a longer time window on the oscilloscope to view target responses. The impedance mismatch at the feedpoint of this antenna is a problem worth further investigation. Although the reflections at this mismatch are now within the system tolerances, this was not the case with the previous antenna. Reflections from its feedpoint caused occasional pulse generator malfunctions. A possible recommended approach to further improve the present impedance mismatch of the monopole is to build a conical outer conductor from the end of the coaxial cable to the image plane that will provide a gradual transition in the impedance. This is discussed in reference 12.

In addition to the transmitting antenna, a satisfactory receiving TEM horn antenna was constructed. Though scattering measurements obtained while using this horn antenna are in agreement with theoretical results, it was felt in later stages of the experimental work that the TEM horn

antenna provided more signal distortion than originally anticipated. This is partially confirmed by the results of the impulse response of the coupled antennas. A thorough experimental analysis is recommended along with a determination of how to optimize signal reception on the image plane.

B. SIGNAL PROCESSING

Enhancing the signal received may be possible with further refinements in the software routine. The program in Appendix A is excellent for initial signal processing. This includes sampling waveform data, incident and augmented signal averaging, and determining target responses. The graphical display presents useful waveform comparisons along with correct statistical data. Although the remainder of the program has been proven to be mathematically correct, the final presentation of the impulse response of a target is polluted with so much noise as to be unusable in most cases. The causes for this should be investigated. One possible cause may be the lack of use of functions such as the Hamming window to reduce aliasing in the FFT's. The signal processing ROM #2 user manual discusses the use of the "TAPER" command in time windowing functions.

C. TARGETS

In addition to the targets already constructed, several other configurations are needed. One example is a large hemisphere made from aluminum. This will serve as a calibration tool in scattering measurements. Another example is a set of bisected cones to match the dimensions of the cones already fabricated. These bisected cones will provide another aspect angle and incident polarization from which to view scattering from this particular geometric configuration.

In general, the targets should be larger in dimension. For some of the original targets, their responses are less than three nanoseconds duration and hence are indistinguishable from noise in the system. Sampling by the DPO should not be a problem related to target resolution because of the high sampling rates used. (25-30 picoseconds/sample). The problem is dependent more on the amplitude of the target response than its duration. Use of the succeeding pulse generator may serve to correct this problem as discussed in Chapter III. Improvements in antenna reception and system noise reduction should also contribute to improved target resolution. This should be an influencing factor in the optimization of the TEM horn antenna.

D. CONCLUDING REMARKS

Future plans for the development of the scattering laboratory include conversion of the antennas from a bistatic system to a monostatic system. The basic monostatic antenna design is patterned from information found in reference 17. It is recommended that a thorough experimental analysis of the transmitting and receiving characteristics of this conical antenna be made prior to any scattering measurements to insure a thorough understanding of the system. It is also recommended, in general, that a complete knowledge of all aspects of the scattering range be understood to insure that a proper interpretation of experimental results is made at all times.

APPENDIX A
Software Program

```
100 INIT
105 DIM A(512),B(512),A1(512),B1(512),C(512)
110 PRINT "ENTER NUMBER OF WAVEFORMS TO BE AVERAGED, N "
120 PRINT
130 INPUT N
140 PRINT
150 PRINT "O.K. N= ";N
160 PRINT "IS IMAGE PLANE PROPERLY SET UP? (TYPE YES WHEN READY) "
170 Y$="YES"
180 INPUT Y$
190 PRINT
200 PRINT "ENTER K=1 FOR INCIDENT AVERAGING, K=2 FOR AUGMENTED AVE."
210 PRINT
220 INPUT K
230 PRINT "O.K. K= ";K
235 PRINT "IF READY TO START, TYPE GO "
240 G$="GO"
250 INPUT G$
260 PAGE
265 REMARK STORE AND HOLD WAVEFORM IN DPO
280 FOR I=1 TO N
300 PRINT @1:"STO ";"A"
310 FOR J=1 TO 30000
315 NEXT J
350 PRINT @1:"HOL ";"A"
355 REMARK TRANSFER WAVEFORM FROM DPO
360 PRINT @1:"CFA?'
370 INPUT @1:A
371 FOR J=1 TO 5
372 IF A(J)<511 THEN 5270
373 NEXT J
380 IF I>1 THEN 400
390 D=0
400 D=D+A
```

```
410 NEXT I
420 IF K=1 THEN 440
430 IF K=2 THEN 460
440 A1=B/N
442 FOR I=256 TO 512
443 A1(I)=511
444 NEXT I
445 A1=A1-511
450 GO TO 480
460 B1=B/N
462 FOR J=256 TO 512
463 B1(J)=511
464 NEXT J
465 B1=B1-511
470 GO TO 530
480 PRINT "INCIDENT WAVEFORM AVERAGING COMPLETED JJ"
490 PRINT "IS TARGET IN POSITION ON IMAGE PLANE? TYPE YES WHEN READY"
500 INPUT Y$
510 K=2
520 GO TO 260
530 PRINT "AUGMENTED WAVEFORM AVERAGING COMPLETED JJ"
540 PRINT "TO COMPUTE INCIDENT WAVEFORM AVERAGE REENTER K=1 J"
545 PRINT "IF RUNS ARE COMPLETE, ENTER K=2 J"
550 INPUT K
560 PRINT "K= ";K
570 IF K=1 THEN 260
580 PAGE
590 REMARK COMPUTE TARGET RESPONSE
600 C=B1-A1
605 GO TO 650
610 FOR I=1 TO 512
620 PRINT I,B1(I),A1(I),C(I)
630 PRINT
640 NEXT I
650 REMARK GRAPHICAL RESULTS
```

```
700 REMARK FIND MAX &MIN VALUES, MEANS, & RMS VALUES
710 A2=1.0E+40
720 A3=-1.0E+40
730 B2=A2
740 B3=A3
750 C2=A2
760 C3=A3
770 FOR I=1 TO 512
780 A2=A1(I) MIN A2
790 A3=A1(I) MAX A3
800 B2=B1(I) MIN B2
810 B3=B1(I) MAX B3
820 C2=C(I) MIN C2
830 C3=C(I) MAX C3
840 NEXT I
850 REMARK GET MEAN VALUES
860 A4=SUM(A1)/512
870 B4=SUM(B1)/512
880 C4=SUM(C)/512
885 REMARK GET RMS VALUES
887 DIM A5(512),B5(512),C5(512),S(512)
890 A5=A1*A1
900 A6=SQR(SUM(A5)/512)
910 B5=B1*B1
920 B6=SQR(SUM(B5)/512)
930 C5=C*C
940 C6=SQR(SUM(C5)/512)
950 PAGE
960 PRINT
970 PRINT "                              WAVEFORM STATISTICS                    "
980 REMARK PLOT INCIDENT AND AUGMENTED WAVEFORMS
985 DIM S(512)
990 R3=A3
1000 R2=A2
1001 R4=A4
```

```
1002 R6=A6
1010 S=A1
1020 GOSUB 4000
1021 A1=S
1022 A2=R2
1023 A3=R3
1024 A4=R4
1025 A6=R6
1030 VIEWPORT 5,60,45,98
1040 GOSUB 5000
1050 DELETE S,R2,R3,R4,R6
1060 DIM S(512)
1070 S=B1
1080 R3=B3
1090 R2=B2
1091 R4=B4
1092 R6=B6
1100 GOSUB 4000
1101 B1=S
1102 B2=R2
1103 B3=R3
1104 B4=R4
1105 B6=R6
1110 VIEWPORT 70,125,45,98
1120 GOSUB 5000
1130 PRINT
1140 PRINT "      INCIDENT                                                  AUGMENTED"
1150 PRINT
1160 PRINT
1170 PRINT "            FOR B- [illegible]
1180 PRINT "                                                    INCIDENT      AUGMENTED"
1190 PRINT
1200 PRINT
1210 IMAGE 3X,30A,2X,3D.4D,5X,3D.4D
1220 PRINT USING 1210:"MAXIMUM PEAK VALUE (VOLTS)",A3,B3
```

```
1230 PRINT
1240 PRINT USING 1210:"MINIMUM VALUE (VOLTS)",A2,B2
1250 PRINT
1260 PRINT USING 1210:"RMS VALUE (VOLTS)",A6,B6
1270 PRINT
1280 PRINT USING 1210:"MEAN VALUE (VOLTS)",A4,B4
1290 PRINT
1300 X$=""
1310 INPUT X$
1320 PAGE
1330 PRINT
1340 PRINT "                              TARGET RESPONSE                    "
1350 C=C*U1
1360 C2=C2*U1
1370 C3=C3*U1
1380 C4=C4*U1
1390 C6=C6*U1
1400 DIM T(512)
1410 FOR I=1 TO 512
1420 T(I)=I*D0
1430 NEXT I
1440 DELETE S,R2,R3,R4,R6
1450 DIM S(512)
1460 S=C
1470 R2=C2
1480 R3=C3
1490 R4=C4
1500 R6=C6
1510 VIEWPORT 25,185,20,90
1520 GOSUB 5000
1530 C=S
1540 C2=R2
1550 C3=R3
1560 C4=R4
1570 C6=R6
```

```
1580 DELETE S,R2,R3,R4,R6
1590 PRINT
1600 PRINT "             FOR N= ";N
1605 PRINT
1610 IMAGE 3X,30A,5X,3D.4D
1620 PRINT USING 1610:"MAXIMUM PEAK VALUE (VOLTS)",C3
1630 PRINT
1640 PRINT USING 1610:"MINIMUM VALUE (VOLTS)",C2
1650 PRINT
1660 PRINT USING 1610:"RMS VALUE (VOLTS)",C6
1670 PRINT
1680 PRINT USING 1610:"MEAN VALUE (VOLTS)",C4
1690 PRINT
1695 X$=""
1700 INPUT X$
1710 PAGE
1720 FOR I=1 TO 512
1730 PRINT T(I),B1(I),A1(I),C(I)
1740 NEXT I
1750 PAGE
1755 REMARK COMPUTE FFT OF INCIDENT WAVEFORM
1756 REMARK COMPUTE FFT OF TARGET RESPONSE
1760 CALL "FFT",A1
1770 CALL "FFT",C
1775 DELETE T,B1
1780 DIM M1(257),P1(257),M2(257),P2(257)
1785 D1=0
1790 CALL "POLAR",A1,M1,P1,D1
1800 CALL "POLAR",C,M2,P2,D1
1810 CALL "MIN",M1,M3,I
1820 CALL "MAX",M1,M4,I
1830 CALL "MIN",M2,M5,I
1840 CALL "MAX",M2,M6,I
1850 CALL "MIN",P1,P3,I
1860 CALL "MAX",P1,P4,I
```

```
1870 CALL "MIN",P2,P5,1
1880 CALL "MAX",P2,P6,1
1890 M7=(M4-M3)/10
1900 M8=(M6-M5)/10
1910 P7=(P4-P3)/10
1920 P8=(P6-P5)/10
1930 PAGE
1940 PRINT
1950 PRINT "         FFT OF INCIDENT AND TARGET WAVEFORMS"
1960 PRINT
1970 WINDOW 0,100,M3,M4
1980 VIEWPORT 5,60,45,90
1990 AXIS 10,M7,0,0
2000 MOVE 0,M1(1)
2010 FOR I=1 TO 100
2020 DRAW I,M1(I)
2030 NEXT I
2040 WINDOW 0,100,P3,P4
2050 VIEWPORT 5,60,5,40
2060 AXIS 10,P7,0,0
2070 MOVE 0,P1(1)
2080 FOR I=1 TO 100
2090 DRAW I,P1(I)
2100 NEXT I
2110 WINDOW 0,100,M5,M6
2120 VIEWPORT 70,125,45,90
2130 AXIS 10,M8,0,0
2140 MOVE 0,M2(1)
2150 FOR I=1 TO 100
2160 DRAW I,M2(I)
2170 NEXT I
2180 WINDOW 0,100,P5,P6
2190 VIEWPORT 70,125,5,40
2200 AXIS 10,P8,0,0
2210 MOVE 0,P2(1)
```

```
2220 FOR I=1 TO 100
2230 READ 1,R(I)
2240 NEXT I
2250 A$=""
2251 T1=C(1,A1(1))
2252 T2=C(2,A1,2)
2253 DELETE C,B1,A1
2260 INPUT N$
2261 DELETE R,I
2262 DIM R(257),I(257)
2263 R(1)=T1
2264 R(257)=T2
2266 DIM M(257),U(257)
2267 I(1)=0
2268 I(257)=0
2280 M=M2/M1
2281 FOR K=101 TO 256
2282 M(K)=0
2283 NEXT K
2290 U=P2-P1
2291 FOR K=101 TO 256
2292 U(K)=0
2293 NEXT K
2310 I(1)=0
2340 FOR J=2 TO 256
2350 R(J)=M(J)*COS(U(J))
2360 I(J)=M(J)*SIN(U(J))
2370 NEXT J
2371 DELETE M,U
2372 DIM Q(512)
2373 REMARK COMPUTE IFT TO FIND IMPULSE RESPONSE
2380 CALL "INLEAV",R,I,Q
2390 CALL "IFT",Q
2400 CALL "MIN",Q,Q1,J
2410 CALL "MAX",Q,Q2,J
```

```
2420 Q3=(Q2-Q1)/10
2430 PAGE
2440 PRINT
2450 PRINT "[illegible] RESPONSE OF TARGET"
2460 PRINT
2470 WINDOW 0,256,Q1,Q2
2480 VIEWPORT 20,110,20,80
2490 AXIS 25.6,Q3,0,0
2500 MOVE 0,Q(1)
2510 FOR J=1 TO 256
2520 DRAW J,Q(J)
2530 NEXT J
2540 HOME
2545 END
2545 CALL "INT",0,0
2547 GO TO 2400
3999 REMARK SUBROUTINE 4000 SCALES DATA FROM DPO
4000 DIM L(80)
4010 PRINT @1:"ADR ";2048
4020 PRINT @1:"DAT?"
4030 INPUT @1:L
4040 L$=""
4050 FOR I=1 TO 80
4060 IF L(I)=127 THEN 4110
4070 IF L(I)=32 THEN 4110
4080 IF L(I)=58 THEN 4110
4090 C$=CHR(L(I))
4100 L$=L$&C$
4110 NEXT I
4120 K1=POS(L$,"V",1)
4130 C$=SEG(L$,1,K1)
4140 K2=LEN(L$)
4150 D$=SEG(L$,K1+1,K2)
4160 V1=VAL(C$)
4170 K1=POS(C$,"V",1)-1
```

```
4180 L$=SEG(C$,K1,1)
4190 U0=POS("munp",L$,1)
4200 U0=181-(3*U0)
4210 U1=P1*U0/102.4
4220 S=S*U1
4221 R2=R2*U1
4222 R3=R3*U1
4223 R4=R4*U1
4224 R6=R6*U1
4230 D0=VAL(D$)
4250 A$=SEG(D$,K1,1)
4260 U0=POS("munp",A$,1)
4270 U0=181-(3*U0)
4280 D0=D0*U0/51.2
4290 RETURN
4999 REMARK SUBROUTINE 5000 PLOTS WAVEFORM DATA
5000 R=R3-R2
5010 R1=1
5020 IF R>10 THEN 5120
5030 R1=0.5
5040 IF R>2 THEN 5120
5050 R1=0.1
5060 IF R>1 THEN 5120
5070 R1=0.05
5080 IF R>0.1 THEN 5120
5090 R1=0.01
5100 IF R>0.1 THEN 5120
5110 R1=0.005
5120 WINDOW 0,256,R2,R3
5130 AXIS 25.6,R1,0,0
5140 MOVE 0,S(1)
5150 FOR I=1 TO 256
5160 DRAW I,S(I)
5170 NEXT I
5175 MOVE 256,R2
```

```
5180 PRINT "[illegible]";
5190 A$=[illegible]"div"
5200 PRINT A$;
5210 MOVE 0,R3
5220 A$=[illegible](P,R1)
5230 A$=A$&"[illegible]div"
5240 PRINT A$;
5250 MOVE 0,P2
5260 RETURN
5270 A(J)=511
5280 GO TO 373
```

APPENDIX B

Target Dielectric Material Specifications

Properties and Applications Data

Dielectric Constant, 60 Hz to 12 GHz	2.54
Loss Tangent, 60 Hz to 10 GHz	0.0005
Homogeneity of Dielectric Constant	± 0.01
Isotropy of Dielectric Constant	∓ 0.01
Volume Resistivity, ohm-om	≥ 1016
Surface Resistivity, ohms/square	1014
Dielectric Strength, volts/mil(Kv/mm)	500(20)
Specific Gravity	1.06
Tensile Strength, psi(Kg/cm^2)	11,000(770)
Flexural Strength, psi(Kg/cm^2)	17,000(1,190)
Modulus of Elasticity, psi(Kg/cm^2)	300,000(21,000)
Izod impact, ft. lbs./in. of notch (Kg-cm/cm)	0.4(2.2)
Coefficient of Linear Expansion/°C (/°F)	$63\text{x}10^{-6}$($35\text{x}10^{-6}$)
Thermal Conductivity, (BTU)(in)/(hr)	0.87
(ft^2)(°F)(cal)(cm)/(sec)(cm^2)(°C)	0.0003
Rockwell Hardness, M Scale	105
Water Absorption, % gain in 24 hrs. at 25°C	0.003
Recommended maximum operating temperature:	
Continuous	125°C(257°F)
Short Time	200°C(392°F)
Recommended minimum operating temperature	-70°C(-94°F)

LIST OF REFERENCES

1. Baum, C.E., "The Singularity Expansion Method", in Topics in Applied Physics, Vol. 10: Transient Electromagnetic Fields, L.B. Felsen, Ed. New York Springer-Verlag, 1976.

2. Pearson, L.W. and Roberson, D.R., "The Extraction of the Singularity Expansion Description of a Scatterer from Sampled Transient Surface Current Response", IEEE Trans. on Antennas & Prop., Vol. AP-28, p. 182-190, March 1980.

3. Kunz, K.S. and Prewitt, J.F., "Practical Limitations to a Natural Mode Characterization of Electromagnetic Transient Response Measurements", IEEE Trans. on Antennas & Prop., Vol. AP-28, p. 575-577, July 1980.

4. Brittingham, J.N., et al., "Pole Extraction from Real Frequency Information", Proceedings of IEEE, Vol. 68, p. 263-273, February 1980.

5. Mei, K.K., Morgan, M.A., Chang, S.K., "Finite Methods in Electromagnetic Scattering", Electromagnetic Scattering, P.L.E. Uslenghi, Ed. New York: Academic Press, 1978.

6. Bennett, C.E., "The Numerical Solution of Transient Electromagnetic Scattering Problems", Electromagnetic Scattering, P.L.E. Uslenghi, Ed. New York: Academic Press, 1978.

7. Schmitt, H.J., "Transients in Cylindrical Antennae", IEE, Vol. 107, Part C, p. 292-298, April 1960.

8. Lamensdorf, D., "The Transient Response of the Coaxial Cone Antenna", IEEE Trans. on Antennas & Prop., Vol. AP-18, No. 6, p. 799-802, November 1970.

9. Tsai, L.L., Hudson, W.T., Brown, G., "Transient Fields Radiated by TEM Horns", IEEE, Amer. Elec. Lab., Atlantic Res. Corp., et al., 1975, International Symposium on EM Compatibility, San Antonio, TX, 7-9 October 1975.

10. Kanda, M., "Transients in a Resistively Loaded Linear Antenna Compared with Those in a Conical Antenna and a TEM Horn", IEEE Trans. on Antennas & Prop., Vol. AP-28, p. 132-136, January 1980.

11. Harrington, R., Time Harmonic Electromagnetic Fields, McGraw-Hill, New York, p. 106-110, 1961.

12. King, R.W.P., The Theory of Linear Antennas, Harvard Univ. Press, Cambridge, Mass., 1956.

13. Liu, T.K. and Mei, K.K., "A Time Domain Integral Equation Solution for Linear Antennas and Scatterers, Radio Science, Vol. 8, p. 797-804, August-September 1973.

14. Mittra, R., "Integral Equation Methods for Transient Scattering", in Topics in Applied Physics, Vol. 10, Transient Electromagnetic Fields, L.B. Felsen, Ed. New York: Springer-Verlag, 1976.

15. Bennett, C.E., Ross, G.F., "Time Domain Electromagnetics and Its Applications", IEEE Proceedings, Vol. 66, No. 3, p. 299-316, March 1978.

16. Sayre, E.P., and Harrington, R., Time Domain Scattering by Thin Wires", Apl. Sci, Res., p. 413-444, September 1972.

17. Miller, E.K., "Validation and Calibration of the LLL Transient Electromagnetic Measurement Facility", Lawrence Livermore Laboratory, Report UCRL-52225, March 1977.

INITIAL DISTRIBUTION LIST

		No. Copies
1.	Defense Technical Information Center Cameron Station Alexandria, Virginia 22314	2
2.	Library, Code 0142 Naval Postgraduate School Monterey, California 93940	2
3.	Department Chairman, Code 62 Department of Electrical Engineering Naval Postgraduate School Monterey, California 93940	1
4.	Professor M. A. Morgan, Code 62Mw) Department of Electrical Engineering Naval Postgraduate School Monterey, California 93940	8
5.	Captain C. W. Hammond, USMC 4614 Spalding Drive Dumfries, Virginia 22026	1

Thesis
H17525 c.1
191459
Hammond
The development of a bistatic electromagnetic scattering laboratory employing time domain measurement techniques for impulse response determination and target classification.